ISSN 1949-8470 (online)

World Journal of *Radiology*

World J Radiol 2023 October 28; 15(10): 281-303

Published by Baishideng Publishing Group Inc

World Journal of Radiology

Contents

Monthly Volume 15 Number 10 October 28, 2023

Contents

ABOUT COVER

Editorial Board Member of *World Journal of Radiology*, Ozum Tuncyurek, Doctor, MD, Associate Professor, Radiology, Near East University Faculty of Medicine, Nicosia 99100, Cyprus. ozum.tuncyurek@gmail.com

AIMS AND SCOPE

The primary aim of *World Journal of Radiology* (*WJR*, *World J Radiol*) is to provide scholars and readers from various fields of radiology with a platform to publish high-quality basic and clinical research articles and communicate their research findings online.

WJR mainly publishes articles reporting research results and findings obtained in the field of radiology and covering a wide range of topics including state of the art information on cardiopulmonary imaging, gastrointestinal imaging, genitourinary imaging, musculoskeletal imaging, neuroradiology/head and neck imaging, nuclear medicine and molecular imaging, pediatric imaging, vascular and interventional radiology, and women's imaging.

INDEXING/ABSTRACTING

The *WJR* is now abstracted and indexed in PubMed, PubMed Central, Emerging Sources Citation Index (Web of Science), Reference Citation Analysis, China National Knowledge Infrastructure, China Science and Technology Journal Database, and Superstar Journals Database. The 2023 Edition of Journal Citation Reports® cites the 2022 impact factor (IF) for *WJR* as 2.5; IF without journal self cites: 2.3; 5-year IF: 2.5; Journal Citation Indicator: 0.54.

RESPONSIBLE EDITORS FOR THIS ISSUE

Production Editor: *Si Zhao*; **Production Department Director:** *Xu Guo*; **Editorial Office Director:** *Jia-Ping Yan.*

NAME OF JOURNAL
World Journal of Radiology

ISSN
ISSN 1949-8470 (online)

LAUNCH DATE
January 31, 2009

FREQUENCY
Monthly

EDITORS-IN-CHIEF
Thomas J Vogl

EDITORIAL BOARD MEMBERS
https://www.wjgnet.com/1949-8470/editorialboard.htm

PUBLICATION DATE
October 28, 2023

INSTRUCTIONS TO AUTHORS
https://www.wjgnet.com/bpg/gerinfo/204

GUIDELINES FOR ETHICS DOCUMENTS
https://www.wjgnet.com/bpg/GerInfo/287

GUIDELINES FOR NON-NATIVE SPEAKERS OF ENGLISH
https://www.wjgnet.com/bpg/gerinfo/240

PUBLICATION ETHICS
https://www.wjgnet.com/bpg/GerInfo/288

PUBLICATION MISCONDUCT
https://www.wjgnet.com/bpg/gerinfo/208

ARTICLE PROCESSING CHARGE
https://www.wjgnet.com/bpg/gerinfo/242

STEPS FOR SUBMITTING MANUSCRIPTS
https://www.wjgnet.com/bpg/GerInfo/239

ONLINE SUBMISSION
https://www.f6publishing.com

World Journal of Radiology

Submit a Manuscript: https://www.f6publishing.com

World J Radiol 2023 October 28; 15(10): 281-292

DOI: 10.4329/wjr.v15.i10.281

ISSN 1949-8470 (online)

ORIGINAL ARTICLE

Retrospective Study

Does the use of computed tomography scenogram alone enable diagnosis in cases of bowel obstruction?

Ozlem Kadirhan, Volkan Kızılgoz, Sonay Aydin, Esra Bilici, Ekrem Bayat, Mecit Kantarci

Specialty type: Radiology, nuclear medicine & medical imaging

Provenance and peer review: Invited article; Externally peer reviewed.

Peer-review model: Single blind

Peer-review report's scientific quality classification

Grade A (Excellent): 0
Grade B (Very good): 0
Grade C (Good): 0
Grade D (Fair): D
Grade E (Poor): 0

P-Reviewer: Ciarambino T, Italy

Received: July 28, 2023
Peer-review started: July 28, 2023
First decision: September 14, 2023
Revised: September 26, 2023
Accepted: October 11, 2023
Article in press: October 11, 2023
Published online: October 28, 2023

Ozlem Kadirhan, Volkan Kızılgoz, Sonay Aydin, Esra Bilici, Ekrem Bayat, Mecit Kantarci, Department of Radiology, Erzincan Binali Yıldırım University, Faculty of Medicine, Erzincan 24000, Turkey

Mecit Kantarci, Department of Radiology, Ataturk University, Faculty of Medicine, Erzurum 25000, Turkey

Corresponding author: Sonay Aydin, MD, Associate Professor, Department of Radiology, Erzincan Binali Yıldırım University, Faculty of Medicine, Haci Ali Akin cd., Erzincan 24000, Turkey. sonay.aydin@erzincan.edu.tr

Abstract

BACKGROUND

Ileus is a pathological condition of the abdomen that presents as a medical emergency. It is characterized by potential complications such as perforation and ischemia, which can lead to significant morbidity and mortality if not promptly addressed. The successful management of ileus relies heavily on the timely and precise identification of the condition. While conventional radiography (CR) is commonly used as the primary diagnostic tool, its accuracy in identifying obstructions ranges from 46% to 80%. Furthermore, the diagnostic accuracy of identifying the location and etiology of intestinal obstruction by CR is limited, therefore making computed tomography (CT) the ideal imaging modality in this regard.

AIM

To determine the presence of acute bowel obstruction (BO) on abdominal CT scenogram images and the accuracy of determining its possible location, taking into account the experience of the observers.

METHODS

A retrospective screening was conducted on an ensemble of 46 individuals who presented to the emergency department between January 2021 and January 2022 with severe abdominal pain and were subsequently monitored for suspected ileus. The abdominal CT scans of these patients were assessed by three radiologists with varying levels of experience (1, 3, and 10 years) at different intervals (1 mo apart). The evaluation focused on determining the presence or absence of BO, as well as identifying the potential location of the obstruction (small bowel or large bowel). The study employed Kappa statistics to assess inter-observer variances, while the McNamer test was used to evaluate obstruction and segmentation discrepancies between observations. A significance level of $P < 0.05$ was determined to indicate statistical significance.

RESULTS

Out of the total sample size of 46 patients, 15 individuals (32.6%) were identified as female, while the remaining 31 individuals (67.4%) were identified as male. The ultimate diagnosis of 42 instances (91.3%) indicated ileus resulting from mechanical obstruction (MO). Among these patients, 14 (33%) experienced obstruction in the large bowel (LB), while 28 (66%) experienced obstruction in the small bowel (SB). The initial evaluation yielded sensitivity rates of 76.19%, 83.31%, and 83.33%, and diagnostic accuracy rates of 69.56%, 76.08%, and 80.43% for the detection of BO among the three observers. The initial study revealed that the average sensitivity of three observers in detecting the presence of ileus caused by MO was 80.94%, while the diagnostic accuracy was 75.35%. Based on the first evaluation, the senior observer demonstrated the highest sensitivity (85.71%), negative predictive value (92.60%), and diagnostic accuracy (80.43%) when accurately estimating the thick and thin segmentation, as per the final diagnosis. There was no statistically significant disparity observed in the sensitivities pertaining to the identification of ileus during the second assessment, as well as the precise determination of the segment level inside the LB or SB, when comparing the second and third observers. Nevertheless, although there was no statistically significant alteration in the detection rate of ileus by the first observer, there was a notable rise in the accuracy rate of segment estimating (73.91%). The senior assessor had a higher level of accuracy in assessing the existence of ileus and segmentation compared to the other evaluators in both evaluations.

CONCLUSION

The findings of our study indicate that the sensitivity and accuracy rates of abdominal CT scenogram scans in diagnosing acute MOs are similar to or greater than those of CR. Additionally, the study revealed that radiologists with more experience demonstrated a higher likelihood of accurately predicting the existence and potential localization of MO compared to their less experienced counterparts.

Key Words: Ileus; Computed tomography; Scenogram scan; Radiography

Core Tip: This retrospective study aims to determine the accuracy of detecting the presence and possible location of obstruction on computed tomography (CT) scenogram images of the abdomen, which can be used as the primary imaging method in the diagnosis of acute bowel obstruction, taking observer experience into account. The experienced observer had the highest sensitivity (83.33%), positive predictive value (94.59%), and diagnostic accuracy (80.43%) for detecting mechanical obstruction (MO). The diagnostic accuracy of the same observer in estimating the segmentation of a MO was 80.43%. These findings show that CT scenogram images alone can demonstrate high diagnostic accuracy and sensitivity in relation to years of experience in diagnosing ileus.

Citation: Kadirhan O, Kızılgoz V, Aydin S, Bilici E, Bayat E, Kantarci M. Does the use of computed tomography scenogram alone enable diagnosis in cases of bowel obstruction? *World J Radiol* 2023; 15(10): 281-292
URL: https://www.wjgnet.com/1949-8470/full/v15/i10/281.htm
DOI: https://dx.doi.org/10.4329/wjr.v15.i10.281

INTRODUCTION

Diagnostic imaging is necessary to determine the existence, location, severity, and potential cause of bowel obstruction (BO) when it is suspected based on clinical indicators and physical examination results[1]. BO is a medical disorder that can arise from either mechanical or functional causes, impeding the regular flow of intestinal contents. The choice of therapy, whether surgical or non-surgical, and subsequent follow-up treatments, will depend on the underlying cause of the obstruction. According to existing literature, it has been reported that around 20% of surgical admissions related to acute abdominal discomfort can be attributed to BO[2]. Timely identification of this condition has significance in terms of averting potential consequences such as perforation and ischemia.

Conventional radiography (CR) is the primary imaging modality utilized for determining the existence of ileus, owing to its widespread availability and cost-effectiveness[3]. Nevertheless, CR is not typically capable of accurately displaying the precise position, extent, and etiology of BO, nor can it effectively identify secondary indications such as aberrant wall thickening, pneumatous acid, and intestinal viability. In contrast, computed tomography (CT) is widely regarded as the preferred modality for addressing these diagnostic needs[4]. The literature has demonstrated a range of 90-95% accuracy for CT in the diagnosis of high-grade intestinal obstructions[5-8]. CT scenogram images are acquired with the patient lying in the supine posture, and they offer a comprehensive overview of the region of interest. These images are obtained with minimal radiation exposure. The utilization of X-rays in both CT and CR imaging techniques results in the generation of ionizing radiation. Ionizing radiation induces heritable alterations in the genetic code *via* deoxyribonucleic acid damage. It has been reported that ionizing radiation can cause cataracts, skin burns, temporary or permanent infertility in the case of exposure to high doses, and various cancers in the case of intermittent exposure to low doses[9]. In a published study, 1012 patients who presented to the emergency department and simultaneously underwent chest X-ray and CT scan were included. This study demonstrated that a single imaging method was able to accurately diagnose the patients in 77.1% of the cases involving trauma and 80.4% of the cases without trauma. Consequently, the prompt referral of patients to appropriate treatment was facilitated, as there was no requirement for a second imaging method. This demonstrates the importance of minimizing the utilization of imaging techniques that include ionizing radiation, in light of the potential adverse consequences[10]. A study revealed that the utilization of CT scenogram images as a standalone diagnostic tool for BO exhibited an interobserver sensitivity ranging from 93% to 86% and a specificity ranging from 85% to 87%. These findings were similar to the outcomes reported for axial CT and the combination of axial and coronal CT[11].

The purpose of this study was to determine the presence and potential location of obstruction on CT scenogram images of the abdomen, which can be used as a primary imaging method in the diagnosis of acute BO, taking observer experience into consideration.

MATERIALS AND METHODS

The research undertaken in this study received approval from the Erzincan University Ethics Committee (Decision no: E-21142744 804.01-128338 Date: December 7, 2021) and was carried out in compliance with the principles outlined in the Declaration of Helsinki.

The retrospective design of the study necessitated the exemption of informed consent. A retrospective investigation was conducted on a cohort of 46 patients who were brought to the emergency department between January 2021 and January 2022. These patients presented with acute abdomen and were subsequently followed up due to suspicion of BO. As part of the evaluation, multi-detector abdominal CT scans were performed. The CT scans underwent anonymization processes and were thereafter uploaded to designated workstations.

The coronal abdominal CT scenogram images of the patients enrolled in the study were assessed by three radiologists who had varying levels of experience, with one having 1 year, another having 3 years, and the third having 10 years of experience. These radiologists were blinded to the final diagnosis of the patients. The abdominal CT scenogram images were assessed at two separate time points, with a one-month interval, to determine the presence of BO (coded as 1 for presence and 0 for absence). Additionally, the localization of the potential obstruction (either in the small bowel or the large bowel) was evaluated in cases where obstruction was suspected.

The ultimate diagnosis was determined by reviewing medical records, surgical reports, and pathology results. The exclusion of BO can be achieved through the identification and treatment of an alternative illness, or by confirming that the patient has not undergone exploratory laparotomy and does not exhibit any indications of prolonged discomfort, abscess, or unexplained fever throughout their hospitalization.

The investigation of inter-observer differences was conducted using Kappa statistics. The percentages of inter-observer and intra-observer agreement were determined by dividing the total number of instances with complete agreement by the overall number of instances. Cohen's Kappa statistics were employed to assess the level of agreement, accounting for the agreement that could occur by chance. Interpretation of the Kappa statistic is as follows: When the value is less than 0.00, the level of agreement is considered poor; when the value falls between 0.00 and 0.20, the agreement is categorized as mild; when the value ranges from 0.21 to 0.40, the agreement is considered fair; when the value falls between 0.41 and 0.60, the agreement is categorized as moderate; when the value ranges from 0.61 to 0.80, the agreement is categorized as considerable; and when the value falls between 0.81 and 1.00, the agreement is virtually perfect. The present study examined the inter-observer appraisal of obstruction and segmentation differences using the McNamer test. The statistical analyses were conducted using the SPSS (Statistical Package for the Social Sciences, SPSS Inc., Chicago, IL, United States) 21.0 software package. Statistical significance was determined by a P value threshold of less than 0.05.

RESULTS

Demographic findings: Out of the total sample size of 46 patients, 15 individuals (32.6%) were identified as female, while the remaining 31 participants (67.4%) were classified as male. The ultimate diagnosis of 42 instances, accounting for 91.3% of the total, indicated ileus resulting from MO. Out of the total number of patients, 14 individuals (33%) exhibited obstruction in the large bowel (LB), whereas 28 individuals (66%) experienced obstruction in the small bowel (SB). A comprehensive breakdown of the factors contributing to obstruction is presented in Table 1. Several case studies are illustrated in Figures 1-4.

The initial assessment scenario for identifying the existence of obstruction: The initial sensitivity findings of the three observers analyzing the abdominal CT scenogram images were 76.19%, 83.31%, and 83.33%, while their diagnostic accuracy results in recognizing the existence of BO were 69.56%, 76.08%, and 80.43%, respectively. The average sensitivity estimate for all three observers in detecting ileus caused by MO during the initial examination was determined to be 80.94%, with a corresponding diagnostic accuracy of 75.35%. The third observer demonstrated the greatest sensitivity (83.33%), positive predictive value (94.59%), and diagnostic accuracy (80.43%) among all observers, as shown in Table 2.

Table 1 Etiologies of cases with mechanical obstruction in this study

Causes of mechanical obstruction	Case count
Postoperative adhesion	**21**
Hernia	**10**
Epigastric	2
Femoral	2
Incisional	1
Indirect inguinal	2
Umbilical	2
Obturator	1
Colon cancer	**6**
Ascending	1
Descending	2
Transverse	1
Sigmoid	2
Volvulus	**3**
Sigmoid	3
Ileitis due to Crohn's disease	**1**
Closed loop obstruction	**1**

Table 2 Observer's concordance with the final diagnosis of obstruction in the scenogram, *n* (%)

	Mechanical obstruction by final diagnosis			Specificity, %	Sensitivity, %	PPV, %	NPV, %	Accuracy, %
	Yes	None	Total					
I Observer								
Yes	32 (76.2)	4 (100)	36 (78.3)	76.19	0	88.88	0	69.56
None	10 (23.8)	0 (0)	10 (21.7)					
II Observer								
Yes	35 (83.3)	4 (100)	39 (84.8)	83.31	0	89.74	0	76.08
None	7 (16.7)	0 (0)	7 (15.2)					
III Observer								
Yes	35 (83.3)	2 (50)	37 (80.4)	83.33	50	94.59	22.23	80.43
None	7 (16.7)	2 (50)	9 (19.6)					
Total	42 (91.3)	4 (8.7)	46 (100)					

Initial examination of obstruction segmentation assessment: Based on the initial evaluation's segmentation according to the final diagnosis, the three observers demonstrated accuracy rates of 54.33%, 65.22%, and 80.43% in estimating the segmentation level of the large and small bowel. Notably, these rates were observed to increase proportionally with the observers' years of experience. In addition, when comparing the results of the 3rd observer with 10 years of experience in accurately evaluating the MO segmentation level to those of the other observers (Table 3), it was seen that this observer had the highest diagnostic sensitivity (85.71%) and negative predictive value (92.60%).

Second assessments: There was no statistically significant distinction observed between the second and third observers in their ability to detect the existence of BO during the second repeated evaluation. Additionally, there was no significant difference in their accuracy in predicting the level of the large or small bowel segment in the presence of obstruction, as well as their sensitivity. The P value obtained was greater than 0.05. Nevertheless, although there was no statistically significant difference in the rate of detecting obstruction by the initial evaluator ($P > 0.05$), there was a noteworthy rise in the rate of accurately estimating segmentation ($P = 0.022$) (Table 4). The diagnostic accuracy for estimating the localization of obstruction segmentation by the first observer increased from 54.33% (Table 3) to 73.91% (Table 6),

Table 3 Concordance of the segmentation diagnoses of the observers with the final diagnosis in the scenogram, *n* (%)

	Mechanical obstruction segment by final diagnosis			Specificity, %	Sensitivity, %	PPV, %	NPV, %	Accuracy, %
	Large	Small	Total					
I Observer								
Large	12 (85.7)	19 (59.4)	31 (67.4)	85.70	40.62	38.67	86.69	54.33
Small	2 (14.3)	13 (40.6)	15 (32.6)					
II Observer								
Large	8 (57.1)	10 (31.3)	18 (39.1)	57.14	68.75	44.40	78.60	65.22
Small	6 (42.9)	22 (68.8)	28 (60.9)					
III Observer								
Large	12 (85.7)	7 (21.9)	19 (41.3)	85.71	78.12	63.12	92.60	80.43
Small	2 (14.3)	25 (78.1)	27 (58.7)					
Total	14 (30.4)	32 (69.6)	46 (100)					

Table 4 Inter-observation agreement of obstruction and segmentation diagnoses in the scenogram in repeat measurements by the observers, *n* (%)

	Observer	Positive predict rate (large)	Negative predict rate (small)	*P* value[a]
Obstruction	I	36 (100)	8 (80)	0.500
	II	35 (89.7)	6 (85.7)	0.375
	III	36 (97.3)	8 (88.9)	0.999
Segmentation	I	20 (64.5)	13 (86.7)	**0.022**
	II	16 (88.9)	23 (82.1)	0.453
	III	18 (94.7)	26 (96.3)	0.999

[a]McNamer test.

Table 5 Concordance of observers' second scenogram obstruction diagnoses with the final diagnosis, *n* (%)

	Mechanical obstruction by final diagnosis			Specificity, %	Sensitivity, %	PPV, %	NPV, %	Accuracy, %
	Yes	None	Total					
I Observer								
Yes	34 (81)	4 (100)	38 (82.6)	81	0	88.47	0	73.91
None	8 (19)	0 (0)	8 (17.4)					
II Observer								
Yes	32 (76.2)	4 (100)	36 (78.3)	76.19	0	88.88	0	69.56
None	10 (23.8)	0 (0)	10 (21.7)					
III Observer								
Yes	35 (83.3)	2 (50)	37 (80.4)	83.33	50	94.59	22.23	80.43
None	7 (16.7)	2 (50)	9 (19.6)					
Total	42 (91.3)	4 (8.7)	46 (100)					

Table 6 Concordance of the segmentation diagnoses of the observers with the final diagnosis in the second scenogram, *n* (%)

	Mechanical obstruction segment by final diagnosis			Specificity, %	Sensitivity, %	PPV, %	NPV, %	Accuracy, %
	Large	Small	Total					
I Observer								
Large	12 (85.7)	10 (31.3)	22 (47.8)	85.71	68.75	54.50	91.68	73.91
Small	2 (14.3)	22 (68.8)	24 (52.2)					
II Observer								
Large	9 (64.3)	12 (37.5)	21 (45.7)	64.29	62.50	42.82	80.03	63.04
Small	5 (35.7)	20 (62.5)	25 (54.3)					
III Observer								
Large	13 (92.9)	6 (18.8)	19 (41.3)	92.86	81.25	68.39	96.30	84.78
Small	1 (7.1)	26 (81.3)	27 (58.7)					
Total	14 (30.4)	32 (69.6)	46 (100)					

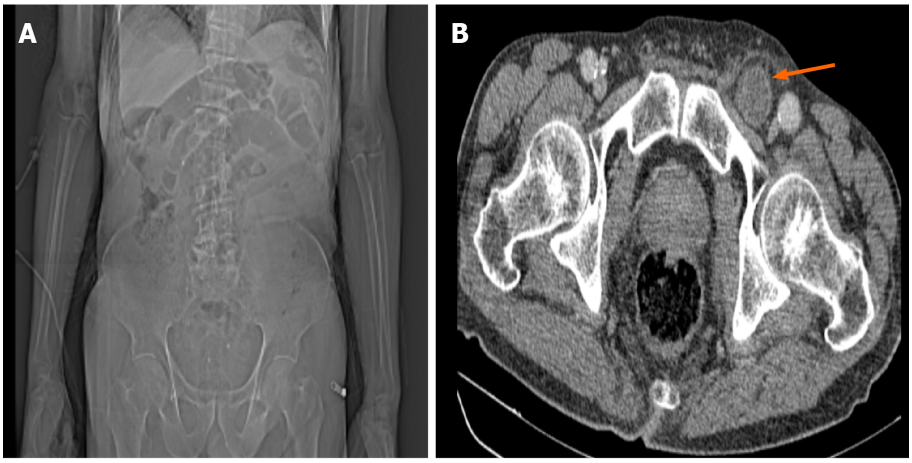

DOI: 10.4329/wjr.v15.i10.281

Figure 1 A 79-year-old male patient admitted to the emergency department with a complaint of abdominal pain that was more pronounced in the left groin. A: Computed tomography (CT) scenogram image shows distension in the small intestine segments; B: Axial CT image shows an incarcerated femoral hernia in the left femoral region (arrow). The first observer, who looked at the scenogram images, reported that there was a possible obstruction at the large intestine level, and the 2nd and 3rd observers reported that there was a possible obstruction at the level of the small intestine.

indicating a noticeable improvement. The accuracy of the 3rd observer in correctly predicting the presence of MO (Table 5) and identifying the potential location of segmentation (Table 6) during the second evaluation was higher compared to the other evaluators.

Intra-rater compliance: Upon evaluation of the Cohen Kappa coefficients pertaining to intra-observer agreement in the diagnosis of MO, it was shown that a moderate level of agreement existed between the first and second observers. Similarly, there was moderate agreement in the diagnosis of obstruction between observers I-III and II-III. The study analyzed Cohen Kappa coefficients to assess the level of agreement among evaluators in diagnosing the potential segmentation location of MO. The results indicated a moderate level of agreement between evaluators I-III and evaluators II-III (P < 0.05). Nevertheless, it was noted that there existed a limited level of concordance between I and II (indicating poor agreement), and it was found that there was no statistically significant evidence of agreement (P = 0.228) (Table 7).

DISCUSSION

BO is a frequently observed clinical condition within the field of general surgery. Failure to urgently diagnose this condition can lead to serious complications, including perforation and ischemia. Therefore, it is of utmost importance to promptly identify and refer patients with suspected small or large BO to the appropriate medical specialty. According to available reports, it has been shown that roughly 75% of mechanical obstructions affecting the gastrointestinal tract are

Table 7 Inter-rater (intra-observation) agreement of the evaluators' diagnoses of obstruction and segmentation on the scenogram, *n* (%)

	Observer	Positive predict rate	Negative predict rate	κ (95%CI)	*P* value
Obstruction	I *vs* II	34 (94.4)	5 (50)	0.498 (0.336-0.660)	0.001
	I *vs* III	33 (91.7)	6 (60)	0.536 (0.382-0.690)	< 0.001
	II *vs* III	35 (95.5)	5 (55.6)	0.548 (0.386-0.710)	< 0.001
Segmentation	I *vs* II	14 (45.2)	11 (73.3)	0.151 (0.03-0.272)	0.228
	I *vs* III	18 (58.1)	14 (93.3)	0.426 (0.314-0.538)	0.001
	II *vs* III	13 (68.4)	22 (81.5)	0.503 (0.373-0.633)	0.001

CI: Confidence interval; κ: Cohen Kappa.

DOI: 10.4329/wjr.v15.i10.281

Figure 2 A 49-year-old male patient admitted to the emergency room with complaints of abdominal pain and vomiting. A: In the computed tomography (CT) scenogram, sudden narrowing at the level of the splenic flexure and distension in the proximal and distal colon loops are seen; B: In the coronal CT image, a mass lesion causing a circular increase in wall thickness is seen at the level of the splenic flexure. All three observers reported a possible obstruction at the level of the large intestine.

specifically localized within the SB[12,13]. In our study, consistent with the literature, there was a predominance of small bowel obstruction (SBO), with a prevalence rate of 66%.

The causes of a MO at the level of the SB can be adhesions, internal and external hernias, primary or extraintestinal neoplasia, stricture due to Crohn's disease, malrotation, duplication cysts, hematoma, ischemic stricture, invagination, endometriosis, and foreign body[14]. Adhesions are commonly identified as the primary cause of MO in western countries, whereas hernias and malignancies are also recognized as significant contributors to this condition[3,15-17]. The total frequency of the aforementioned three etiologies exceeds 80%[18]. In our research, the underlying causes of obstruction occurring in the SB were primarily attributed to surgical adhesions, with external hernias being the second most prevalent factor.

The causes of MO at the level of the LB include colorectal cancer, diverticulitis, volvulus, stricture owing to Crohn's disease, non-colorectal malignancy, endometriosis, ischemic stenosis, hernia, adhesions, fecal impaction, and foreign body[13,19]. Over 60% of cases of colonic obstruction are caused by colon malignancies[2,20], with the sigmoid colon and splenic flexure being the most prevalent locations[21]. In our study, the most common cause among the etiologies of colon involvement was colon cancer, and the most common location was the sigmoid colon. Volvulus is the second most common (10%-15%) cause of LBO. The second most frequent (10%–15%) cause of obstruction of the LB is volvulus. Volvulus is observed at low frequencies (< 1%) at the transverse colon and splenic flexure levels, but at high rates in the colon at the sigmoid (60%-75%) and cecum (25%-33%) levels[2,5]. According to our study, volvulus, which is localized at the sigmoid colon level, is the second most frequent cause of MO in the LB.

Anamnesis and physical exam results by themselves are insufficient for diagnosis and appropriate guidance; in cases of suspected BO, evaluation in conjunction with imaging techniques is crucial. However, depending on the extent of BO, diagnosis might be challenging even with advancements in abdominal imaging[22]. BO can be diagnosed using a variety of radiological modalities, including barium exams, enteroclysis, CT, ultrasound, and CR.

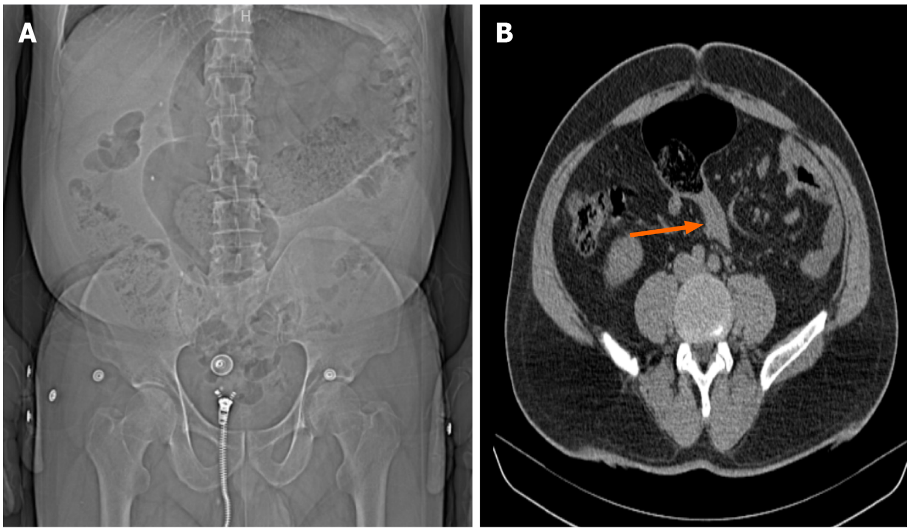

DOI: 10.4329/wjr.v15.i10.281 **Copyright** ©The Author(s) 2023.

Figure 3 A 56-year-old male patient admitted to the emergency department with complaints of abdominal pain, gas and inability to pass stool. A: In the computed tomography (CT) scanogram, swelling in the midline of the abdomen and folds in the colon loops are seen; B: In the coronal CT image, narrowing in the lower transition zones secondary to sigmoid volvulus is observed (arrow). All three observers reported a possible obstruction at the level of the large intestine.

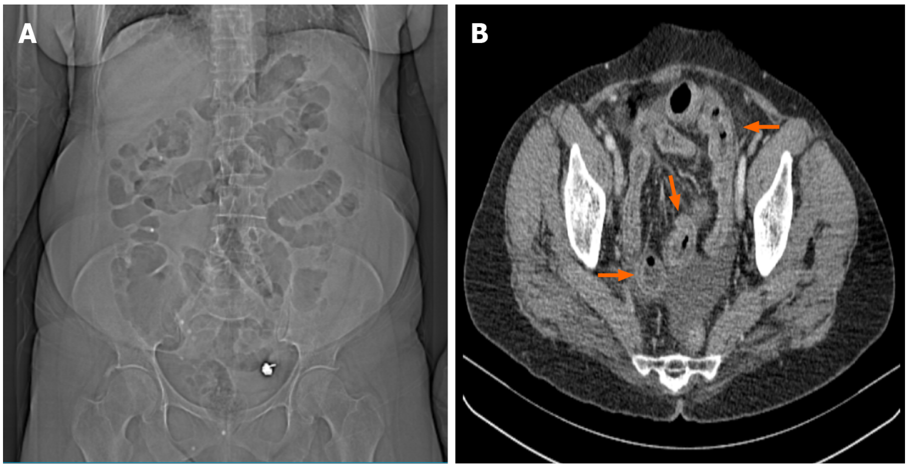

DOI: 10.4329/wjr.v15.i10.281 **Copyright** ©The Author(s) 2023.

Figure 4 A 61-year-old female patient admitted to the emergency department complaining of abdominal pain. A: Radiolucent air values in the large and small intestine segments are seen in the computed tomography (CT) scenogram image; B: Axial CT image shows trilaminar thickness increase (red arrows) in the small intestine wall compatible with ileitis, dilated appearance in the mesenteric vascular structures and free fluid in the pelvic area. Following observation of the scenogram images, the first observer reported a possible obstruction at the small intestine level, the second observer reported a possible obstruction at the large intestine level, and the third observer reported that no mechanical obstruction was detected.

In patients presenting with abdominal pain and suspected BO, the primary objective of imaging is to detect possible obstruction, and CR is the first preferred imaging modality due to its low cost and low radiation exposure. The literature reports the diagnostic accuracy of CR for detecting BO to range from 46%-80%[3] and its sensitivity has been shown to range from 19%-86%[3,16,23]. The observed proportional difference may be attributed to variations in the severity of obstruction among the patients included in the studies.

CT is indicated for patients presenting with suspected BO in cases where the patient's clinical symptoms and initial CR findings are inconclusive. In order to effectively manage early treatment in cases of ileus, it is crucial to accurately determine the localization, etiology, severity of obstruction, transition point, and the presence of additional findings such as abnormal wall thickening, pneumatosis, strangulation, and pneumoperitoneum within the affected intestinal segment. Therefore, the utilization of a CT scan is imperative in order to validate the diagnosis and ascertain supplementary observations in contrast to CR[4]. CT has been documented to have a high diagnostic sensitivity (94%-100%) and diagnostic accuracy (90%-95%) for determining the presence and severity of complete or high-grade BO[24]. The diagnostic precision of CT is diminished when there is incomplete low-grade or intermittent obstruction. In such instances, enteroclysis and CT enteroclysis are the preferred approaches for assessing the existence and severity of BO[7].

In addition to established imaging techniques employed in CT, localizer radiographs, also referred to as scout, topogram, or scenogram images, and are acquired to facilitate identification of the initial and final positions of the scanning range. These radiographs rely on the anatomical landmarks of the patients to accurately determine the desired scan area[25]. CT scenogram images are a valuable contemporary implementation of conventional abdominal radiography. They serve the purpose of identifying supplementary information that aids in making a direct diagnosis of specific pathologies or narrowing down the differential diagnosis. This is achieved by examining findings both within and outside the scanned field of view. CT scenogram images can be utilized to assess many entities, including foreign substances (such as those that are undesirable, characterized by devices, or localized within the body), air-related findings (such as bowel gas pattern, pneumoperitoneum, and pneumatosis), calcifications, trauma/bone-related concerns, as well as soft tissues[26,27]. However, there have been reports indicating that scenogram images are eliminated from CT scanning examinations at a frequency of up to 75%, or alternatively, they are disregarded by a majority of radiologists when interpreting CT examinations[28-30]. In this study, the presence and possible location of the obstruction on abdominal CT scenograms, which can be used as the primary imaging modality in the diagnosis of acute BO, were contrasted with the final diagnosis, taking the observer's experience into account. There is only one study in the literature that examines the diagnostic accuracy of CT scenogram images in BO by different observers, taking into account the periods of experience. The diagnostic sensitivity reported in this study varies from 93% to 86%, with an average of 88%. These findings demonstrate a similarity to the results obtained for axial and axial plus coronal CT within the same investigation[11]. In our study, the evaluators' ability to accurately detect the existence of MO through the assessment of CT scenogram images exhibited a range of sensitivity values, spanning from 76.19% to 83.33%. The average sensitivity for diagnostic purposes was determined to be 80.94%.

The CT scenogram images can be classified into two categories based on the patterns of intestinal gas: Obstructive patterns and non-obstructive patterns. Imaging modalities of mechanical BO typically indicate decompressed loops in the distal region of the obstruction, as well as abnormally expanded bowel loops in the proximal region of the obstruction. Similar, imaging findings are present at levels showing distension on CT scenogram images. Supine CR images have characteristic findings expected in BO. The expected findings in an obstruction at the level of SB segments are enlarged air- or liquid-filled intestine with a diameter greater than 2.5-3 cm, colorectal gas deficiency, enlarged stomach, gasless abdomen, stretch sign, SB enlargement disproportionate to the colon, pseudotumor sign, *etc.* LBO is characterized by enlarged air- or liquid-filled bowel segments greater than 9 cm in the cecum and 6 cm in other levels of the colon, rectal gas deficiency, and SB dilatation, which may sometimes be accompanied by check valve system disorder[18]. These characteristic findings can also be identified in CT scenogram images.

Closed loop obstructions arise as a result of many factors such as adhesions, internal hernias, congenital malformations, or iatrogenic mesenteric deformities. These obstructions specifically affect a distinct segment and involve nearby sites of obstruction. In these instances, there exists a potential hazard of ischemia and necrosis resulting from total occlusion. While CT scenogram images may exhibit distinctive indicators of SBOs, similar to CRs, the proximal segment typically displays less tension and the closed loop segment tends to contain fluid, resulting in a normal or "non-specific" appearance on imaging[31].

Sigmoid volvulus refers to an abnormal bending of the sigmoid colon along its mesenteric axis, being the predominant type of colonic volvulus with a prevalence ranging from 60%-75% of cases[32]. In CT scenogram images, the characteristic inverted U-shaped swollen sigmoid colon pointing to the right upper quadrant seen on CRs, disproportionate sigmoid distension, proximal colon dilatation, absence of rectal gas or dilated sigmoid colon cephalo extension above the transverse colon (northern exposure), and sigmoid findings such as the 'coffee bean' sign describing the distandual segment with central coated walls can be identified[33,34]. It has been reported that an inverted U-shape can be seen in 86%-94% of cases[33,35] and the "coffee bean" sign can be seen in 76% of cases[33] in CT scenogram images.

Abdominal CT scans are frequently employed in the evaluation of patients who present with abdominal pain and are thought to have BO. These scans are commonly used to identify specific abnormalities, such as pneumoperitoneum and pneumatosis, which serve as indicators of the existence of severe or extensive obstruction. The evaluation of pneumoperitoneum presents challenges when using supine radiographs. In cases where there is suspicion, chest radiographs are primarily employed as they have the capability to detect even small amounts of intraperitoneal gas, as little as 1 mL[36]. The assessment of pneumoperitoneum is more challenging when using supine radiographs. However, several subtle features have been documented that could potentially indicate the existence of pneumoperitoneum. These findings are typically observed on CT scenogram images. These findings are: Rigler sign, right upper quadrant gas sign, falciform ligament sign, football sign, and inverted V sign[37,38]. Pneumatosis intestinalis is the presence of gas in the intestinal wall, and it is a warning sign for ischemia and impending perforation in the event of BO[32]. Pneumatosis typically appears as gas accumulation in the lower part of the intestine, whereas pseudopneumatosis refers to the entrapment of gas inside the stool's wall. This condition can provide a resemblance to genuine pneumatosis when observed using abdominal radiography or CT scenogram images. However, distinguishing between pseudopneumatosis and actual pneumatosis is more effectively achieved through the use of CT scans[39]. Portal venous gas is an additional indication of possible ischemia resulting from BO, which can be shown on CRs in situations of significant severity[40]. In our study, there were no cases with perforation-pneumoperiteneum, ischemia-pneumatosis findings secondary to severe MO.

The scarcity of research in the existing body of literature regarding the diagnosis of BO and the determination of the potential obstructed segment using CT scenogram images is evident. The insufficient attention provided by radiologists to these factors, together with their correlation to seniority level, underscores the significance of this research.

The retrospective nature of this study, the small number of patients, and the fact that, despite the high diagnostic accuracy of the results reported by the observers, they failed to provide clear indications of the criteria upon which they based their estimates constituted limitations. Other limitations of CT scenogram images include limited resolution, supine positioning, and two-dimensional planar presentation of complex three-dimensional anatomy. In addition, the fact that the female/male ratio is not suitable statistically for the comparison of parameters between genders is another limitation of this study. As the symptom and anamnesis information of most of the cases included in the study was not accessible, the evaluation was carried out mainly and only on radiological images. Incorporating clinical information into the evaluation process may alter study data.

CONCLUSION

This study revealed that the sensitivity and accuracy rates for detecting the presence and segmentation of MO on abdominal CT scenogram images were comparable to or greater than those observed in CR, particularly in relation to the radiologist's level of experience. While scenogram images are typically not given much attention during CT scans and are often disregarded by radiologists during interpretation, it is crucial to examine and incorporate any relevant data from CT scenogram images into the diagnostic report.

ARTICLE HIGHLIGHTS

Research background

The effective management of ileus is heavily reliant on prompt and precise diagnosis, as a failure to achieve this may lead to adverse health outcomes and potential loss of life. While conventional radiography (CR) is commonly used as the primary imaging modality for patients with a preliminary diagnosis of ileus, its diagnostic accuracy in identifying the specific site and underlying cause of bowel obstruction (BO) is limited. Due to this constraint, computed tomography (CT) has emerged as the most suitable imaging modality in this particular situation.

Research motivation

CT scenogram images have the potential to assess several entities, encompassing air-related observations such as intestinal gas pattern, pneumoperitoneum, and pneumatosis. However, there are reports showing that scenogram images are omitted from CT scan examinations up to 75% of the time, or alternatively, ignored by the majority of radiologists when interpreting CT examinations. There exists a singular study within the literature that investigates the diagnostic sensitivity of CT scans in detecting BO, specifically considering the varying levels of expertise among different observers. Our intention was to make a scholarly contribution within this particular field of study.

Research objectives

This study aims to determine the presence of acute BO on abdominal CT scenogram images and the accuracy with which its possible location can be determined, taking into account the experience of the observers.

Research methods

A retrospective screening was performed on a group of 46 people who arrived at the emergency room with acute abdominal pain between January 2021 and January 2022 and were subsequently evaluated for suspected ileus. The patients' abdominal CT images were evaluated at different intervals (1 mo apart) by three radiologists with varying degrees of expertise (1, 3, and 10 years). The assessment focused on establishing the presence or absence of BO as well as the likely location of the obstruction (small bowel or large bowel).

Research results

In the first evaluation by 3 radiologists to detect the presence of BO, the rate of detecting the presence of ileus due to mechanical obstruction (MO) was 80.94% and the diagnostic accuracy was 75.35%. Among all observers, the third observer had the highest sensitivity (83.33%), positive predictive value (94.59%), and diagnostic accuracy (80.43%). Considering the segmentation according to the final diagnosis at the first evaluation, the sensitivity (85.71%) and diagnostic accuracy (80.43%) values were highest in the senior observer's correct estimation of the large and small bowel segmentation. In the second evaluation, the senior observer's prediction of the presence of ileus and segmentation was more accurate than the other observers. Compared to the second evaluation, while there was no significant change in the rate of the first observer detecting the presence of ileus, there was an increase in the rate of correctly predicting the segmentation (73.91%). No significant change was detected in the other observers' estimates of the presence of MO and possible localization at different periods.

Research conclusions

Our results show that the sensitivity and accuracy of abdominal CT scenogram images in detecting the presence and segmentation of acute MO in relation to seniority is similar to or higher than CR.

Research perspectives

Considering the possible contribution of CT scenogram images to the diagnosis of some pathologies such as ileus, more studies are needed to diagnose these and similar pathologies and to narrow down the differential diagnosis.

FOOTNOTES

Author contributions: Kadirhan O, Kızılgoz V, Aydin S, Bilici E, Bayat E, Kantarci M contributed to conceptualization, validation, formal analysis, resources, data curation; Kadirhan O, Kızılgoz V, and Aydin S contributed to methodology, investigation, writing – original draft preparation, writing – review & editing, visualization, supervision; Kadirhan O and Aydin S contributed to project administration.

Institutional review board statement: The research undertaken in this study received approval from the Erzincan University Ethics Committee (Decision no: E-21142744 804.01-128338 Date: 07/12/ 2021) and was carried out in compliance with the principles outlined in the Declaration of Helsinki.

Informed consent statement: As the study was designed retrospectively, no written informed consent form was obtained from patients.

Conflict-of-interest statement: All the authors have no conflicts of interest to declare.

Data sharing statement: Participants approved publication of their data after anonymization.

Country/Territory of origin: Turkey

ORCID number: Ozlem Kadirhan 0000-0003-2175-084X; Volkan Kızılgoz 0000-0003-3450-711X; Sonay Aydin 0000-0002-3812-6333; Esra Bilici 0009-0007-9983-8901; Ekrem Bayat 0000-0003-1335-4839; Mecit Kantarci 0000-0002-1043-6719.

S-Editor: Liu JH
L-Editor: Webster JR
P-Editor: Liu JH

REFERENCES

1 **Herlinger H**, Rubesin SE, Morris JB. Small bowel obstruction. In: Gore RM, Levine MS, editors. Textbook of gastrointestinal radiology. 2nd ed. Philadelphia, Pa: Saunders; 2000; 815–837 [DOI: 10.1016/b978-1-4160-2332-6.50055-5]

2 **Welch JP**. Bowel obstruction: differential diagnosis and clinical management. 1987 [DOI: 10.1001/jama.1990.03450030118046]

3 **Maglinte DD**, Reyes BL, Harmon BH, Kelvin FM, Turner WW Jr, Hage JE, Ng AC, Chua GT, Gage SN. Reliability and role of plain film radiography and CT in the diagnosis of small-bowel obstruction. *AJR Am J Roentgenol* 1996; **167**: 1451-1455 [PMID: 8956576 DOI: 10.2214/ajr.167.6.8956576]

4 **Liu P**, Zhu H, Zhang X, Feng A, Zhu X, Sun Y. Predicting Survival for Hepatic Arterial Infusion Chemotherapy of Unresectable Colorectal Liver Metastases: Radiomics Analysis of Pretreatment Computed Tomography. *J Transl Int Med* 2022; **10**: 56-64 [PMID: 35702189 DOI: 10.2478/jtim-2022-0004]

5 **Gore RM**, Miller FH, Pereles FS, Yaghmai V, Berlin JW. Helical CT in the evaluation of the acute abdomen. *AJR Am J Roentgenol* 2000; **174**: 901-913 [PMID: 10749221 DOI: 10.2214/ajr.174.4.1740901]

6 **Maglinte DD**, Heitkamp DE, Howard TJ, Kelvin FM, Lappas JC. Current concepts in imaging of small bowel obstruction. *Radiol Clin North Am* 2003; **41**: 263-283, vi [PMID: 12659338 DOI: 10.1016/s0033-8389(02)00114-8]

7 **Suri S**, Gupta S, Sudhakar PJ, Venkataramu NK, Sood B, Wig JD. Comparative evaluation of plain films, ultrasound and CT in the diagnosis of intestinal obstruction. *Acta Radiol* 1999; **40**: 422-428 [PMID: 10394872 DOI: 10.3109/02841859909177758]

8 **Balthazar EJ**. George W. Holmes Lecture. CT of small-bowel obstruction. *AJR Am J Roentgenol* 1994; **162**: 255-261 [PMID: 8310906 DOI: 10.2214/ajr.162.2.8310906]

9 **Karavas E**, Ece B, Aydın S, Kocak M, Cosgun Z, Bostanci IE, Kantarci M. Are we aware of radiation: A study about necessity of diagnostic X-ray exposure. *World J Methodol* 2022; **12**: 264-273 [PMID: 36159099 DOI: 10.5662/wjm.v12.i4.264]

10 **Fatihoglu E**, Aydin S, Gokharman FD, Ece B, Kosar PN. X-ray Use in Chest Imaging in Emergency Department on the Basis of Cost and Effectiveness. *Acad Radiol* 2016; **23**: 1239-1245 [PMID: 27426978 DOI: 10.1016/j.acra.2016.05.008]

11 **Jaffe TA**, Martin LC, Thomas J, Adamson AR, DeLong DM, Paulson EK. Small-bowel obstruction: coronal reformations from isotropic voxels at 16-section multi-detector row CT. *Radiology* 2006; **238**: 135-142 [PMID: 16293807 DOI: 10.1148/radiol.2381050489]

12 **Markogiannakis H**, Messaris E, Dardamanis D, Pararas N, Tzertzemelis D, Giannopoulos P, Larentzakis A, Lagoudianakis E, Manouras A, Bramis I. Acute mechanical bowel obstruction: clinical presentation, etiology, management and outcome. *World J Gastroenterol* 2007; **13**: 432-437 [PMID: 17230614 DOI: 10.3748/wjg.v13.i3.432]

13 **Drożdż W**, Budzyński P. Change in mechanical bowel obstruction demographic and etiological patterns during the past century: observations from one health care institution. *Arch Surg* 2012; **147**: 175-180 [PMID: 22351915 DOI: 10.1001/archsurg.2011.970]

14 **Sabiston DC**, Townsend CM, Beauchamp R, Evers BM, Mattox KL. Sabiston textbook of surgery: the biological basis of modern surgical practice: Wb Saunders Philadelphia; 2001 [DOI: 10.1007/s10350-008-9293-5]

15 **Jeffrey RB**. Small bowel obstruction. In: Federle MP, Jeffrey RB, Woodward PJ, Borhani AA, eds. Diagnostic imaging: abdomen, 2nd ed. Salt Lake City, Utah: Amirsys, 2010; 44–47 [DOI: 10.2214/ajr.142.1.91]

16 **Frager DH**, Baer JW. Role of CT in evaluating patients with small-bowel obstruction. *Semin Ultrasound CT MR* 1995; **16**: 127-140 [PMID: 7794603 DOI: 10.1016/0887-2171(95)90005-5]

17 **Miller G**, Boman J, Shrier I, Gordon PH. Etiology of small bowel obstruction. *Am J Surg* 2000; **180**: 33-36 [PMID: 11036136 DOI: 10.1016/s0002-9610(00)00407-4]

18 **Paulson EK**, Thompson WM. Review of small-bowel obstruction: the diagnosis and when to worry. *Radiology* 2015; **275**: 332-342 [PMID: 25906301 DOI: 10.1148/radiol.15131519]

19 **Cappell MS**, Batke M. Mechanical obstruction of the small bowel and colon. *Med Clin North Am* 2008; **92**: 575-597, viii [PMID: 18387377 DOI: 10.1016/j.mcna.2008.01.003]

20 **Biondo S**, Parés D, Frago R, Martí-Ragué J, Kreisler E, De Oca J, Jaurrieta E. Large bowel obstruction: predictive factors for postoperative mortality. *Dis Colon Rectum* 2004; **47**: 1889-1897 [PMID: 15622582 DOI: 10.1007/s10350-004-0688-7]

21 **Garcia-Valdecasas JC**, Llovera JM, deLacy AM, Reverter JC, Grande L, Fuster J, Cugat E, Visa J, Pera C. Obstructing colorectal carcinomas. Prospective study. *Dis Colon Rectum* 1991; **34**: 759-762 [PMID: 1914740 DOI: 10.1007/bf02051066]

22 **Matrawy KA**, El-Shazly MJAJom. Intestinal obstruction: role of multi-slice CT in emergency department. 2014; 50: 171-178 [DOI: 10.1016/j.ajme.2014.01.005]

23 **Shrake PD**, Rex DK, Lappas JC, Maglinte DD. Radiographic evaluation of suspected small bowel obstruction. 1991; 86 [DOI: 10.53347/rid-149375]

24 **Boudiaf M**, Soyer P, Terem C, Pelage JP, Maissiat E, Rymer R. Ct evaluation of small bowel obstruction. *Radiographics* 2001; **21**: 613-624 [PMID: 11353110 DOI: 10.1148/radiographics.21.3.g01ma03613]

25 American Association of Physicists in Medicine. AAPM CT Lexicon version 1.3. 2012

26 **Lee MH**, Lubner MG, Mellnick VM, Menias CO, Bhalla S, Pickhardt PJ. The CT scout view: complementary value added to abdominal CT interpretation. *Abdom Radiol (NY)* 2021; **46**: 5021-5036 [PMID: 34075469 DOI: 10.1007/s00261-021-03135-3]

27 **Bian Y**, Jiang H, Zheng J, Shao C, Lu J. Basic Pancreatic Lesions: Radiologic-pathologic Correlation. *J Transl Int Med* 2022; **10**: 18-27 [PMID: 35702187 DOI: 10.2478/jtim-2022-0003]

28 **Daffner RH**. Reviewing CT Scout Images: Observations of an Expert Witness. *AJR Am J Roentgenol* 2015; **205**: 589-591 [PMID: 26295646 DOI: 10.2214/AJR.15.14405]

29 **Berlin L**. Reviewing the CT scout view: medicolegal and ethical considerations. *AJR Am J Roentgenol* 2014; **202**: 1264-1266 [PMID: 24848823 DOI: 10.2214/AJR.12.10444]

30 **Berlin L**. Medicolegal--malpractice and ethical issues in radiology. CT scout views and standard of care. *AJR Am J Roentgenol* 2014; **203**: W741 [PMID: 25415741 DOI: 10.2214/AJR.14.13442]

31 **Balthazar EJ**, Birnbaum BA, Megibow AJ, Gordon RB, Whelan CA, Hulnick DH. Closed-loop and strangulating intestinal obstruction: CT signs. *Radiology* 1992; **185**: 769-775 [PMID: 1438761 DOI: 10.1148/radiology.185.3.1438761]

32 **Jaffe T**, Thompson WM. Large-Bowel Obstruction in the Adult: Classic Radiographic and CT Findings, Etiology, and Mimics. *Radiology* 2015; **275**: 651-663 [PMID: 25997131 DOI: 10.1148/radiol.2015140916]

33 **Levsky JM**, Den EI, DuBrow RA, Wolf EL, Rozenblit AM. CT findings of sigmoid volvulus. *AJR Am J Roentgenol* 2010; **194**: 136-143 [PMID: 20028915 DOI: 10.2214/AJR.09.2580]

34 **Javors BR**, Baker SR, Miller JA. The northern exposure sign: a newly described finding in sigmoid volvulus. *AJR Am J Roentgenol* 1999; **173**: 571-574 [PMID: 10470881 DOI: 10.2214/ajr.173.3.10470881]

35 **Burrell HC**, Baker DM, Wardrop P, Evans AJ. Significant plain film findings in sigmoid volvulus. *Clin Radiol* 1994; **49**: 317-319 [PMID: 8013194 DOI: 10.1016/s0009-9260(05)81795-7]

36 **James B**, Kelly B. The abdominal radiograph. *Ulster Med J* 2013; **82**: 179-187 [PMID: 24505155]

37 **Menuck L**, Siemers PT. Pneumoperitoneum: importance of right upper quadrant features. *AJR Am J Roentgenol* 1976; **127**: 753-756 [PMID: 973660 DOI: 10.2214/ajr.127.5.753]

38 **Levine MS**, Scheiner JD, Rubesin SE, Laufer I, Herlinger H. Diagnosis of pneumoperitoneum on supine abdominal radiographs. *AJR Am J Roentgenol* 1991; **156**: 731-735 [PMID: 2003436 DOI: 10.2214/ajr.156.4.2003436]

39 **Wang JH**, Furlan A, Kaya D, Goshima S, Tublin M, Bae KT. Pneumatosis intestinalis versus pseudo-pneumatosis: review of CT findings and differentiation. *Insights Imaging* 2011; **2**: 85-92 [PMID: 22347936 DOI: 10.1007/s13244-010-0055-2]

40 **Liebman PR**, Patten MT, Manny J, Benfield JR, Hechtman HB. Hepatic--portal venous gas in adults: etiology, pathophysiology and clinical significance. *Ann Surg* 1978; **187**: 281-287 [PMID: 637584 DOI: 10.1097/00000658-197803000-00012]

World Journal of Radiology

Submit a Manuscript: https://www.f6publishing.com

World J Radiol 2023 October 28; 15(10): 293-303

DOI: 10.4329/wjr.v15.i10.293

ISSN 1949-8470 (online)

ORIGINAL ARTICLE

Retrospective Study

Two-point Dixon and six-point Dixon magnetic resonance techniques in the detection, quantification and grading of hepatic steatosis

Mohamed Elfaal, Alanna Supersad, Craig Ferguson, Stephanie Locas, Florin Manolea, Mitchell P Wilson, Medica Sam, Wendy Tu, Gavin Low

Specialty type: Radiology, nuclear medicine and medical imaging

Provenance and peer review: Unsolicited article; Externally peer reviewed.

Peer-review model: Single blind

Peer-review report's scientific quality classification

Grade A (Excellent): A
Grade B (Very good): 0
Grade C (Good): 0
Grade D (Fair): 0
Grade E (Poor): 0

P-Reviewer: Ji G, China

Received: September 6, 2023
Peer-review started: September 6, 2023
First decision: September 19, 2023
Revised: September 20, 2023
Accepted: September 28, 2023
Article in press: September 28, 2023
Published online: October 28, 2023

Mohamed Elfaal, Alanna Supersad, Craig Ferguson, Stephanie Locas, Florin Manolea, Mitchell P Wilson, Medica Sam, Wendy Tu, Gavin Low, Department of Radiology & Diagnostic Imaging, University of Alberta, Edmonton T6G2B7, Alberta, Canada

Corresponding author: Gavin Low, MBChB, MPhil, MRCS, FRCR, Professor, Department of Radiology & Diagnostic Imaging, University of Alberta, WMC 2B2.41 8440-112 ST, Edmonton T6G2B7, Alberta, Canada. gavinlow@mic.ca

Abstract

BACKGROUND

Hepatic steatosis is a very common problem worldwide.

AIM

To assess the performance of two- and six-point Dixon magnetic resonance (MR) techniques in the detection, quantification and grading of hepatic steatosis.

METHODS

A single-center retrospective study was performed in 62 patients with suspected parenchymal liver disease. MR sequences included two-point Dixon, six-point Dixon, MR spectroscopy (MRS) and MR elastography. Fat fraction (FF) estimates on the Dixon techniques were compared to the MRS-proton density FF (PDFF). Statistical tests used included Pearson's correlation and receiver operating characteristic.

RESULTS

FF estimates on the Dixon techniques showed excellent correlation (≥ 0.95) with MRS-PDFF, and excellent accuracy [area under the receiver operating characteristic (AUROC) ≥ 0.95] in: (1) Detecting steatosis; and (2) Grading severe steatosis, ($P < 0.001$). In iron overload, two-point Dixon was not evaluable due to confounding T2* effects. FF estimates on six-point Dixon *vs* MRS-PDFF showed a moderate correlation (0.82) in iron overload *vs* an excellent correlation (0.97) without iron overload, ($P < 0.03$). The accuracy of six-point Dixon in grading mild steatosis improved (AUROC: 0.59 to 0.99) when iron overload cases were excluded. The excellent correlation (> 0.9) between the Dixon techniques *vs* MRS-PDFF did not change in the presence of liver fibrosis ($P < 0.01$).

CONCLUSION

Dixon techniques performed satisfactorily for the evaluation of hepatic steatosis but with exceptions.

Key Words: Chemical shift encoded Dixon magnetic resonance techniques; Hepatic steatosis; Liver fat quantification; Magnetic resonance spectroscopy; Proton density fat fraction; Ultrasound

Core Tip: Fat fraction (FF) estimates on the Dixon techniques (two-point Dixon and six-point Dixon) have excellent correlation with magnetic resonance spectroscopy-proton density FF (MRS-PDFF), and excellent accuracy in detecting steatosis, and grading severe steatosis. However, in iron overload, two-point Dixon was not evaluable due to confounding effect on liver signal from T2* decay. The excellent correlation between the Dixon techniques *vs* MRS-PDFF was not affected by co-existing liver fibrosis.

Citation: Elfaal M, Supersad A, Ferguson C, Locas S, Manolea F, Wilson MP, Sam M, Tu W, Low G. Two-point Dixon and six-point Dixon magnetic resonance techniques in the detection, quantification and grading of hepatic steatosis. *World J Radiol* 2023; 15(10): 293-303
URL: https://www.wjgnet.com/1949-8470/full/v15/i10/293.htm
DOI: https://dx.doi.org/10.4329/wjr.v15.i10.293

INTRODUCTION

Non-alcoholic fatty liver disease (NAFLD) is the most common chronic liver disease worldwide with a global prevalence of 25% (estimated at 1 billion people)[1-5]. Roughly 20% have non-alcoholic steatohepatitis (NASH), characterized by hepatocyte injury and inflammation. These patients are at risk for progression to liver fibrosis and cirrhosis[6]. Consequently, steatosis and fibrosis may frequently co-exist in the liver. NAFLD is also associated with metabolic syndrome, type 2 diabetes and cardiovascular disease[6]. Accurate detection, quantification and grading of steatosis are necessary for risk stratification, to monitor disease progression and to assess the treatment response.

Liver biopsy is the reference standard for liver fat evaluation but is invasive and can be associated with pain, bleeding and death (1 in 10000)[7]. It has poor patient acceptability and is not suitable as a screening tool or for longitudinal patient monitoring. Biopsy is associated with high sampling variability as it only evaluates 1:50000th of the liver[8]. As steatosis often affects the liver non-uniformly, biopsy may be poorly representative. Finally, the histopathology assessment is a qualitative process prone to intra- and inter-reader variability[7].

B-mode ultrasound (US) is the first-line imaging test for investigating patients with suspected parenchymal liver disease. It is non-invasive, easy to perform, inexpensive and widely available. However, it has questionable utility as a screening tool due to poor sensitivity in mild steatosis[1,6,9]. Magnetic resonance spectroscopy (MRS) is widely regarded as the non-invasive reference standard for liver fat quantification. It is strongly correlated with histopathology and has been touted as a replacement for biopsy[10-12]. It can directly measure the chemical composition of liver fat and produces a proton density fat fraction (PDFF) according to the formula: PDFF = F/(F + W), where F and W are the unconfounded signals of protons within mobile fat and mobile water molecules, respectively. MRS has drawbacks including a limited spatial coverage and is technically demanding requiring specialized software and expertise so is generally only available in large academic centers.

Chemical shift encoded fat and water separation MR techniques are based on the principle that fat and water protons oscillate at different resonant frequencies. The fat-water resonance frequency differences (225 Hz at 1.5 T and 450 Hz at 3 T) create phase shifts that can be used to separate fat and water signals. The first chemical shift fat and water separation method, termed ‘two-point Dixon’, was described in 1984[13]. This technique involves the dual-echo acquisition of T1 weighted in-phase (IP) and opposed-phased (OP) images that can be used to generate separated fat-only and water-only images. This allows the hepatic FF to be calculated as follows[6]: FF% = (IP - OP)/(2 × IP). Two-point Dixon sequences are part of the routine toolkit of MR liver imaging worldwide, and have been performed in many clinical applications over the years. These are familiar sequences to practicing body MR radiologists, easy to perform, can sample large areas of the liver, and do not require sophisticated software. However, 1st generation fat quantification on two-point Dixon is prone to underestimation due to confounders such as B_0 inhomogeneity, T1 bias, T2* effects, noise bias, spectral complexity of fat, eddy currents and J-coupling[6]. Fat quantification is also adversely affected by liver iron overload due to T2* decay which has opposing effects to fat on liver signal leading to inaccuracies. Additionally, the two-point Dixon technique has a narrower dynamic range of 0%-50% liver FF although this approximates the normal biologic range in humans so is not generally a practical limitation[1,14]. Recent advances have led to the development of modern Dixon sequences that are corrected for confounders leading to more accurate liver fat quantification[1,14,15]. These complex multi-echo chemical shift encoded techniques utilize both the phase and magnitude of the MR signal and can provide fat quantification [MR imaging (MRI)-PDFF] over the entire physical range (0%-100%). The most common method involves the acquisition of 6 echos and is termed ‘six-point Dixon’. By performing automatic segmentectomy, multi-echo Dixon techniques can generate whole liver fat quantification. Confounder corrected R2* maps, acquired simultaneously, provide fat-corrected liver iron quantification. Unlike two-point Dixon which is performed ubiquitously in clinical liver imaging worldwide, six-point Dixon requires dedicated software that has to be purchased separately, so access to this technique is limited clinically.

On this background, the primary aim of this study was to assess the diagnostic performance of 1st generation two-point Dixon (widely available clinically) and modern six-point Dixon MR techniques (limited access clinically) in the detection, quantification and grading of hepatic steatosis, using MRS as the reference standard. The secondary aims were: (1) To assess the confounding effects of iron overload on the Dixon techniques, a subgroup analysis was performed in patients with and without iron overload; (2) As steatosis and fibrosis are often found together in NAFLD patients, a subgroup analysis was performed to determine if liver fibrosis had an influence on FF estimates; and (3) To assess the accuracy of US for detecting and grading hepatic steatosis, a subgroup analysis was performed in patients with an US examination within 6 mo of the MR.

MATERIALS AND METHODS

This was a retrospective single-center cross-sectional study. Institutional ethics and review board approval was granted and the requirement for informed patient consent was waived. From July 2021 to February 2022 (8 mo), all consecutive adult patients (≥ 18 years old) that underwent a per-protocol clinical MR examination for the combined assessment of liver fat, iron and fibrosis for suspected diffuse parenchymal liver disease and without known focal liver lesions, were entered into the study. Three patients were excluded from the study due to technically poor-quality MR examinations.

MR protocol

All examinations were performed on a 1.5-T MR system (Magnetom Aera, Siemens Healthcare, Erlangen, Germany) using an 18-channel body matrix array coil. The technical MR parameters are included in Table 1. Additionally, an MR elastography (MRE) examination was also performed using a commercially available clinical system (Resoundant, MN, United States).

Data processing and analysis

For the MR examination, the proprietary liver fat and iron quantification software (LiverLab, Siemen Healthcare) automatically generates the following information on picture archiving and communication system (PACS): (1) A report of the mean MRI-PDFF (%) and mean R2* (s^{-1}) of the entire liver (segmentectomy) and of a selected region of interest (ROI); and (2) A spectroscopy report of the mean MRS-PDFF (%) of a 27 cm^3 voxel. The MRI-PDFF (segmentectomy) and MRS-PDFF data as well as liver stiffness data acquired on MRE were imported into an Excel spreadsheet. Only the primary investigative team (Mohamed Elfaal and Alanna Supersad) had access to this data.

After removing patient identifying information, the following anonymized datasets were entered into 1 of 2 research folders on PACS. Cases were randomized within each folder and allocated unique research identification numbers. Folder 1 contained the T1 IP and OP MR images (two-point Dixon) of all patients. Folder 2 contained the static and cine US images of patients with an US within 6 mo of the MR. Three fellowship trained board-certified radiologists (with 2 years, 2 years, and 5 years of clinical experience, respectively) independently analyzed cases in folder 1. The readers were blinded to the clinical data. Using a well-established and validated technique, each reader manually placed 4 circular ROIs over the liver (2 in each hepatic lobe) on both the T1 IP and OP MR images[16]. The ROI size was set to a minimum threshold of 4 cm in diameter/12.6 cm^2 area and ROIs were placed taking care to avoid large vessels, bile ducts and the liver margin. The hepatic FF on two-point Dixon was calculated using the formula[6], FF = (IP - OP)/(2 × IP).

Three other fellowship trained board-certified radiologists (with 3 years, 4 years, and 2 years of clinical experience, respectively) independently analyzed cases in folders 2. The readers were blinded to the background clinical data. For folder 2, the readers were required to assess if hepatic steatosis was present or absent on the US images, and determine the grade of steatosis. The following US criteria were used[17,18]: (1) Mild steatosis: Liver echogenicity exceeds that of the renal cortex; (2) Moderate steatosis: Poor delineation of the echogenic walls of the intrahepatic portal vein branches; and (3) Severe steatosis: Loss of definition of the posterior hepatic margin or diaphragm outline.

Reader data on folders 1 and 2 were submitted to the primary investigative team for export into the excel spreadsheet. For folder 1, a group averaged FF on two-point Dixon was calculated for each case. For folder 2, the group decision on whether steatosis was present or absent on each case was determined by the majority rule. Cases that did not meet agreement by at least 2 of the 3 readers were not included in the final analysis.

Sample size calculation

An a-prior power analysis was performed on G* Power. Assuming a mild effect size of 0.4, alpha of 0.05 and beta of 0.2, a minimum sample size of 52 was needed to achieve a power of 0.8.

Statistical analysis

The following statistical tests were used: (1) Intraclass correlation coefficient (ICC) to calculate the inter-reader agreement for FF estimates on two-point Dixon; (2) Pearson's correlation and Bland Altman to assess the inter-test correlation and variability, respectively, for FF estimates on two-point Dixon *vs* MRS, and six-point Dixon *vs* MRS; (3) Linear regression to model the relationship between two-point Dixon *vs* MRS, and six-point Dixon *vs* MRS for fat quantification; (4) Receiver operating characteristic (ROC) analysis to determine the accuracy of two-point Dixon, six-point Dixon and US

Table 1 Acquisition parameters for the magnetic resonance sequences

	Two-point Dixon	Six-point Dixon	MRS
TR (ms)	6.68	15.6	3000
TE (ms)	2.39, 4.77	2.38, 4.76, 7.14, 9.52, 11.90, 14.28	12, 24, 36, 48, 72
Flip angle	10°	4°	90°
Matrix size	288 mm × 176 mm	160 mm × 97 mm	N/A[1]
FOV (mm)	400	450	N/A[1]
Bandwidth (kHz/pixel)	470	1080	1200
Slice thickness (mm)	3	3.5	N/A[1]
NSA	1	1	1
Parallel imaging, acceleration factor	CAIPIRINHA 2	CAIPIRINHA 4	-

[1]Magnetic resonance spectroscopy was performed on a 30 mm × 30 mm × 30 mm voxel.

FOV: Field of view; NSA: Number of signal averages; MRS: Magnetic resonance spectroscopy; TR: Time to repetition; TE: Time to echo; N/A: Not applicable.

for the detection and grading of steatosis; and (5) Fleiss kappa to calculate the inter-reader agreement for detecting steatosis on US. The kappa (k) value interpretation as suggested by Cohen was used: $k < 0.20$ (poor agreement), 0.21-0.40 (fair agreement), 0.41-0.60 (moderate agreement), 0.61-0.80 (good agreement), and 0.81-1.00 (excellent agreement)[19].

Statistical analysis was performed on IBM SPSS (version 26) and MedCalc (version 19.6.1). A P value of < 0.05 was considered statistically significant. Statistical review was performed by a study author with training in medical statistics.

RESULTS

There were 62 patients including 33 males (53.2%) and 29 females (46.8%). The mean age was 54.4 ± 13.2 years and ranged from 18 to 80 years. Past medical history included obesity in 23 (37.1%), diabetes in 16 (25.8%), dyslipidemia in 15 (24.2%), hypertension in 14 (22.6%), NASH in 3 (4.8%), NAFLD in 2 (3.2%), hepatitis B in 1 (1.6%), hepatitis C in 1 (1.6%) and hypothyroidism in 1 (1.6%). The body mass index (BMI) was available in 33 patients (53.2%) with a mean BMI of 34.7 ± 7.8 kg/m^2 (range 19.8-60.4 kg/m^2). Accordingly, 25 (40.3%) were obese (BMI ≥ 30 kg/m^2) and 6 (9.7%) were overweight (BMI 25-29.9 kg/m^2).

The mean MRS-PDFF was 13.6% ± 8.9% (range 2.6%-34.3%). As proposed by Starekova *et al*[6], PDFF thresholds for mild, moderate and severe hepatic steatosis were set as 5%, 15% and 25%, respectively. Using MRS-PDFF as the reference standard, mild steatosis was found in 23 (37.1%), moderate steatosis in 15 (24.2%), severe steatosis in 9 (14.5%), and a non-steatotic liver in 15 (24.2%).

Seven patients (11.3%) had hepatic iron overload - all were of mild grade. This was associated with a mean R2* of 88.2 ± 21.7 s^{-1} (range 70.4-133.3 s^{-1}) and a mean liver iron concentration of 2.8 ± 2.8 mg/g Fe$_{dw}$ (range 2.2-4.4 mg/g Fe$_{dw}$). The FF was not evaluable on two-point Dixon in any of these patients as T2* effects from iron led to net signal loss on the IP images relative to the OP images resulting in erroneously negative calculations using the FF formula. The 7 cases were removed from the two-point Dixon dataset so the resulting dataset (n = 55) consisted of only cases with a normal liver iron concentration (< 2 mg/g Fe$_{dw}$). In contrast, six-point Dixon was not failed by iron overload and this dataset (n = 62) included a mixed cohort of cases with and without iron overload.

The liver stiffness was acquired in 60 patients and not evaluable in two others due to technical failure of MRE. A liver stiffness cut-off of ≥ 2.9 Ka was used to indicate the presence of liver fibrosis (F1 or higher)[20]. Accordingly, there were 24 patients (36.9%) with liver fibrosis and 36 patients (55.4%) without liver fibrosis.

ICC showed an excellent inter-reader agreement of 0.99 [95% confidence interval (CI): 0.99-1, P < 0.001] for calculating the FF estimates on two-point Dixon. Pearson showed an excellent inter-test correlation of 0.95 and 0.96, respectively, for FF estimates on two-point Dixon *vs* MRS-PDFF and six-point Dixon *vs* MRS-PDFF, P < 0.001. On six-point Dixon *vs* MRS-PDFF, a moderate correlation (0.82) was noted in iron overload *vs* an excellent correlation (0.97) without iron overload, P < 0.03. In comparison, liver fibrosis did not affect the correlation between FF estimates and the MRS-PDFF. Excellent correlations of 0.98 (fibrosis) *vs* 0.98 (no fibrosis) on two-point Dixon and 0.92 (fibrosis) *vs* 0.94 (no fibrosis) on six-point Dixon were noted, P < 0.01.

Bland Altman was used to assess the inter-test variability of FF estimates on the Dixon techniques *vs* MRS-PDFF (Figures 1 and 2). The mean difference between tests and 95% lower and upper limits of agreement (LOA) were: (1) 1.2% and -6.1%, 8.5% on two-point Dixon *vs* 0.8% and -4.3%, 5.9% on six-point Dixon; (2) 1.5% and -9.5%, 12.5% (iron overload) *vs* 0.7% and -3.3%, 4.7% (no iron overload), on six-point Dixon; (3) 1.5% and -3.9%, 5.4% (liver fibrosis) *vs* 1.1% and -7.4%, 9.5% (no liver fibrosis), on two-point Dixon; and (4) 0.7% and -3%, 4.5% (liver fibrosis) *vs* 0.9% and -5%, 6.8% (no liver fibrosis), on six-point Dixon.

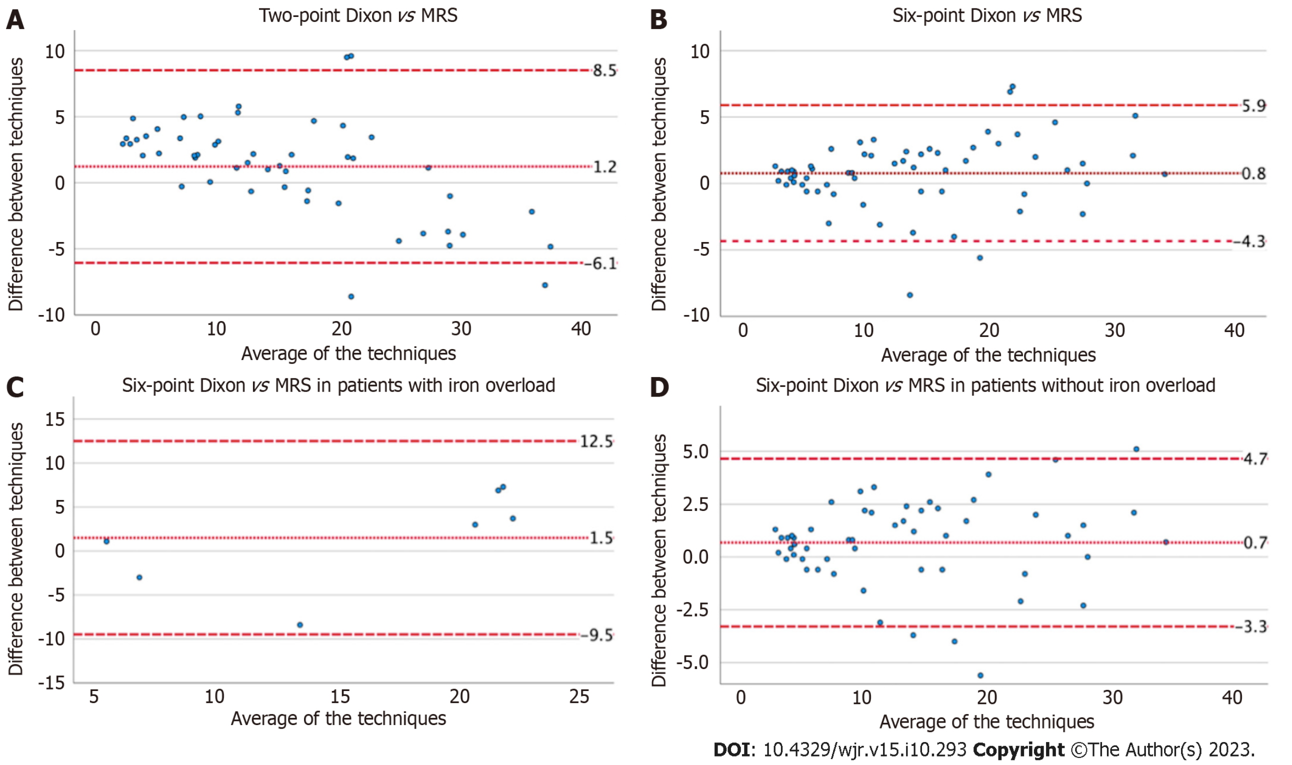

Figure 1 Bland Altman plots demonstrate the inter-test variability for fat fraction estimates. A: Two-point Dixon *vs* magnetic resonance spectroscopy (MRS); B: Six-point Dixon *vs* MRS; C and D: Patients with and without liver iron overload on six-point Dixon *vs* MRS. MRS: Magnetic resonance spectroscopy.

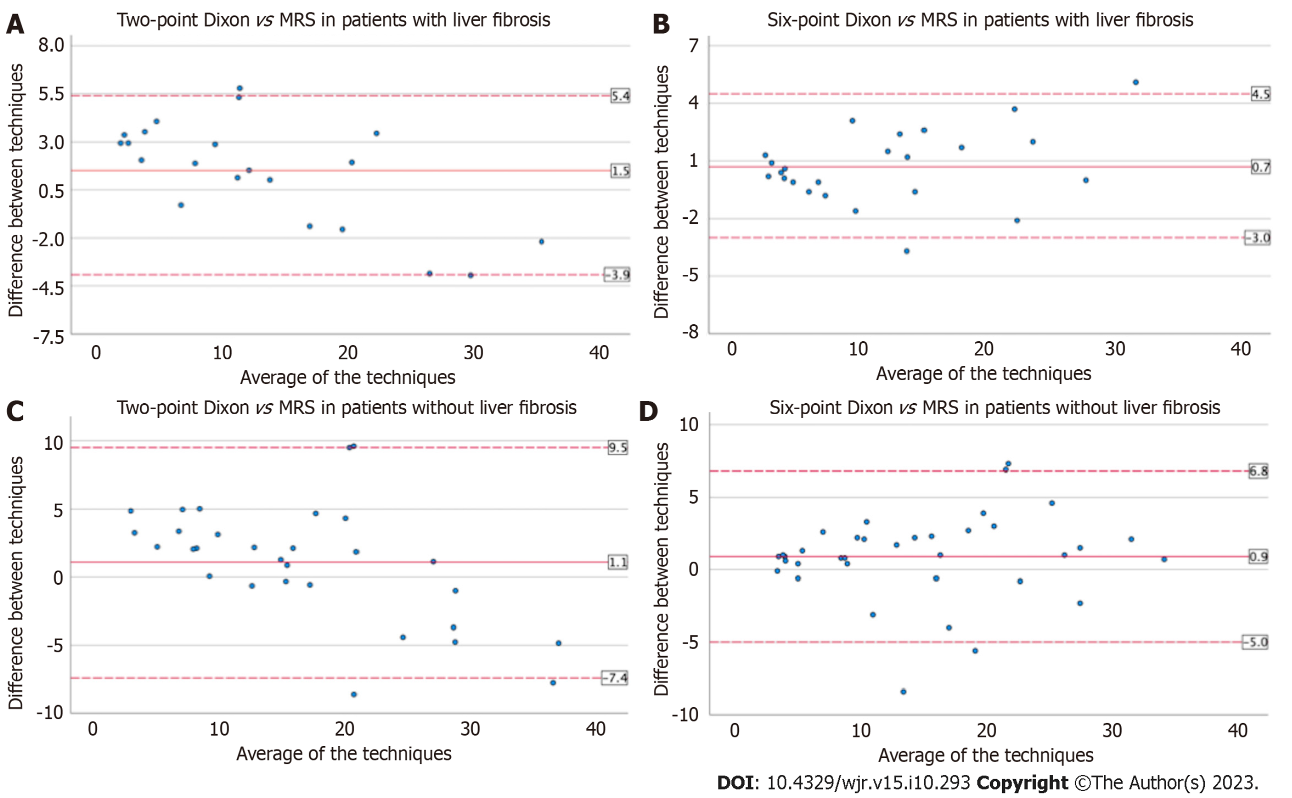

Figure 2 Bland Altman plots demonstrate the inter-test variability for fat fraction estimates *vs* magnetic resonance spectroscopy for patients with and without liver fibrosis on two-point Dixon and six-point Dixon. A: Two-point Dixon *vs* magnetic resonance spectroscopy (MRS) in patients with liver fibrosis; B: Six-point Dixon *vs* MRS in patients with liver fibrosis; C: Two-point Dixon *vs* MRS in patients without liver fibrosis; D: Six-point Dixon *vs* MRS in patients without liver fibrosis. MRS: Magnetic resonance spectroscopy.

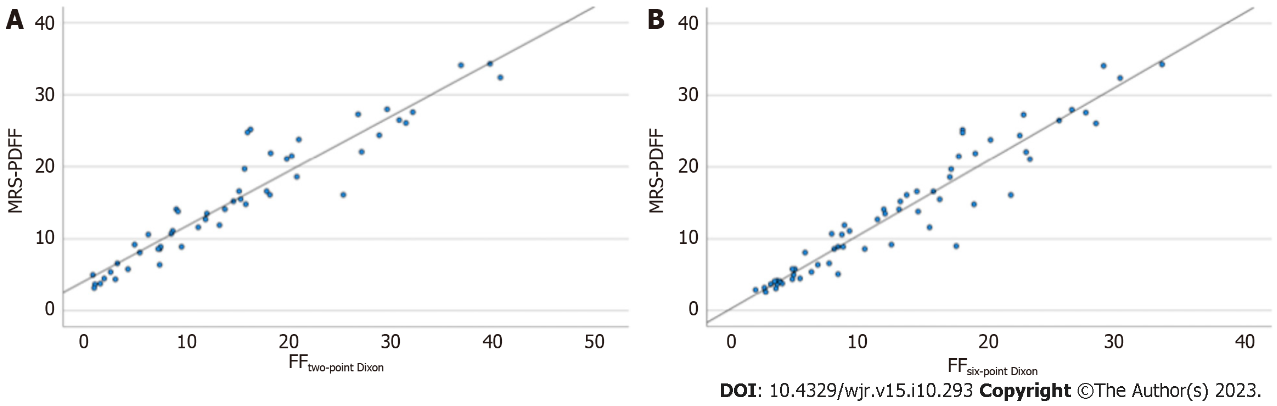

Figure 3 Scatterplots demonstrate a strong linear relationship. A: Scatterplots demonstrate a strong linear relationship between two-point Dixon *vs* magnetic resonance spectroscopy (MRS); B: Scatterplots demonstrate a strong linear relationship between six-point Dixon *vs* MRS for liver fat quantification. MRS: Magnetic resonance spectroscopy; PDFF: Proton density fat fraction.

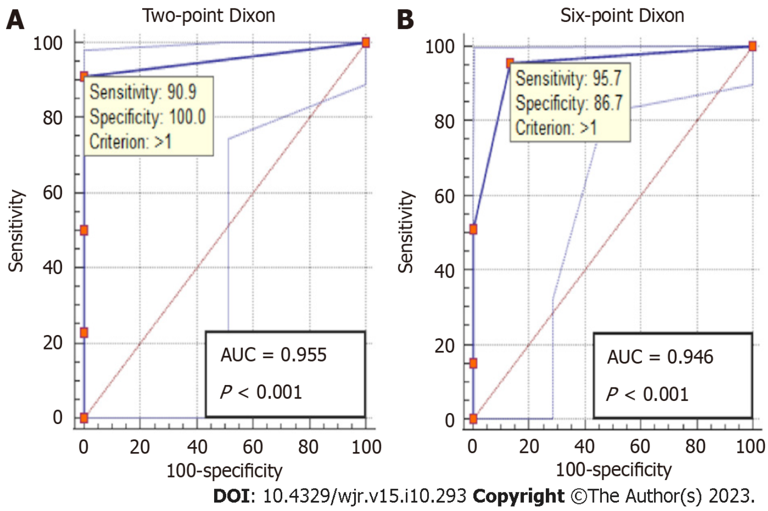

Figure 4 Receiver operating characteristic analysis demonstrates excellent accuracy for detecting hepatic steatosis on two-point Dixon and six-point Dixon. A: Two-point Dixon; B: Six-point Dixon. AUC: Area under the curve.

Linear regression showed a highly significant linear relationship between the Dixon techniques and MRS for liver fat quantification (P < 0.001) (Figure 3). For two-point Dixon, the regression equation was: MRS-PDFF (%) = 4.67 + 0.76 ($FF_{\text{two-point Dixon}}$). The R^2 was 0.90 signifying that 90% of the variance in MRS-PDFF was predictable from the FF estimates on two-point Dixon. For six-point Dixon, the regression equation was: MRS-PDFF (%) = 0.59 + 1.02 ($FF_{\text{six-point Dixon}}$). The R^2 was 0.92 signifying that 92% of the variance in MRS-PDFF was predictable from the FF estimates on six-point Dixon.

ROC analysis showed an excellent accuracy for detecting steatosis on both two-point Dixon [area under the ROC (AUROC) = 0.96, 95%CI: 0.86-0.99, P < 0.001] and six-point Dixon (AUROC = 0.95, 95%CI: 0.86-0.99, P < 0.001) (Figure 4). Similarly, an excellent accuracy was found for grading severe steatosis on both two-point Dixon (AUROC = 0.96, 95%CI: 0.87-1, P < 0.001) and six-point Dixon (AUROC = 0.97, 95%CI: 0.89-1, P < 0.001) (Figure 5). For grading moderate steatosis, there was fair accuracy on both two-point Dixon (AUROC = 0.72, 95%CI: 0.58-0.84, P = 0.001) and six-point Dixon (AUROC = 0.75, 95%CI: 0.62-0.85, P < 0.001). For grading mild steatosis, the accuracy was fair on two-point Dixon (AUROC = 0.75, 95%CI: 0.61-0.86, P < 0.01) but poor on six-point Dixon (AUROC = 0.59, 95%CI: 0.46-0.71, P = 0.21). When patients with iron overload were removed from the analysis, the accuracy for grading mild steatosis increased to excellent on six-point Dixon (AUROC = 0.99, 95%CI: 0.91-1.00, P < 0.001) (Figure 6A).

There were 29 patients that had an US examination within 6 mo of the MR. Fleiss kappa found a moderate inter-reader agreement (k = 0.45, 95%CI: 0.33-0.58, P < 0.001) for detecting steatosis on US. For grading steatosis, the inter-reader agreement was moderate for both mild steatosis (k = 0.44, 95%CI: 0.23-0.65, P < 0.001) and severe steatosis (k = 0.42, 95%CI: 0.21-0.63, P < 0.001), and fair for moderate steatosis (k = 0.28, 95%CI: 0.10-0.49, P = 0.01). Conversely, the inter-reader agreement for detecting a non-steatotic liver on US was excellent (k = 0.82, 95%CI: 0.61-1, P < 0.001). ROC analysis demonstrated that US had a good accuracy for detecting steatosis (AUROC = 0.86, 95%CI: 0.67-0.96, P < 0.001) but was inferior in grading steatosis. US showed poor accuracy in grading mild steatosis (AUROC = 0.62, 95%CI: 0.41-0.80, P = 0.27) and only fair accuracy in grading both moderate steatosis (AUROC = 0.79, 95%CI: 0.59-0.93, P < 0.001) and severe steatosis (AUROC = 0.78, 95%CI: 0.58-0.92, P < 0.01) (Figures 6B and 7).

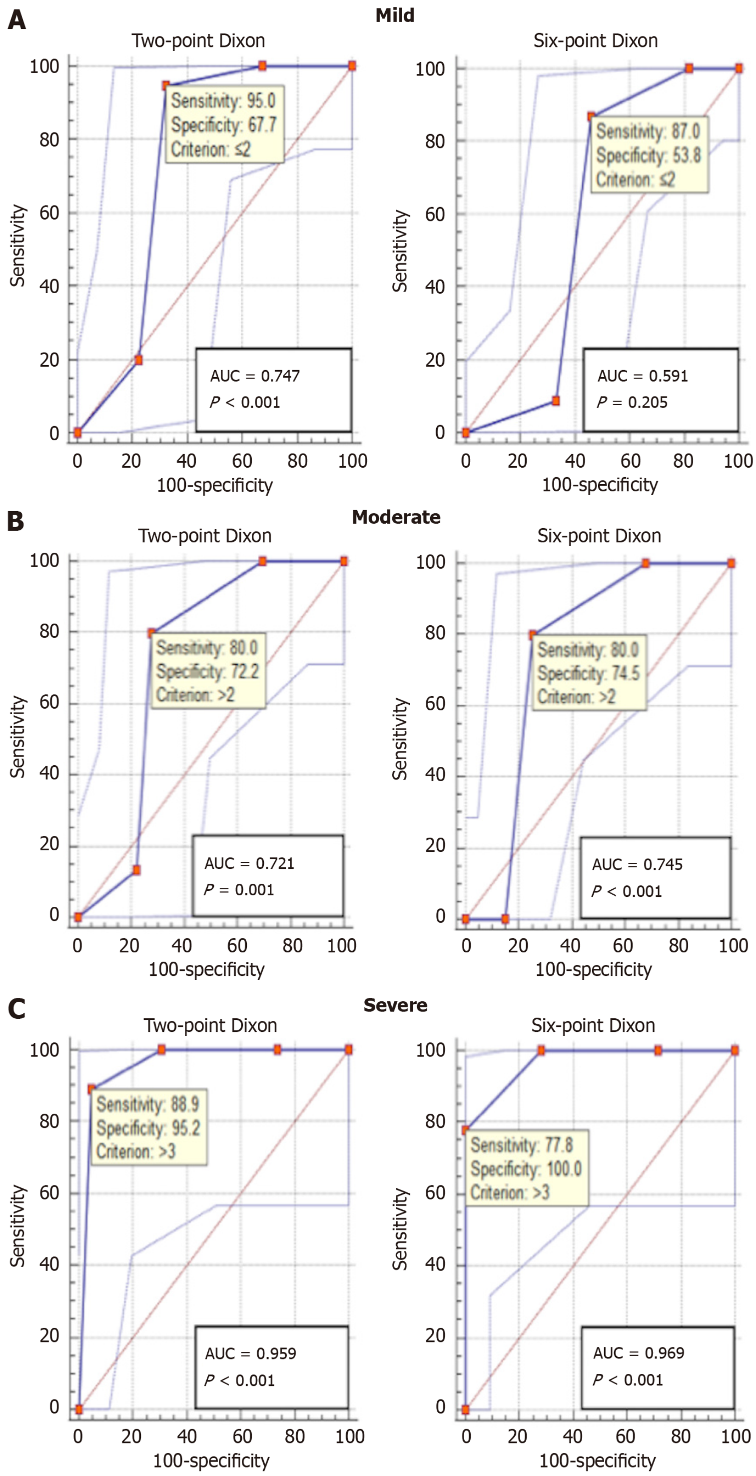

Figure 5 Receiver operating characteristic analysis. A: The accuracy for grading mild hepatic steatosis on two-point Dixon and six-point Dixon; B: The accuracy for grading moderate hepatic steatosis on two-point Dixon and six-point Dixon; C: The accuracy for grading severe hepatic steatosis on two-point Dixon and six-point Dixon. Two-point Dixon was performed in patients with no iron overload while six-point Dixon was performed in a mixed cohort of patients with and without iron overload. AUC: Area under the curve.

DISCUSSION

MRS-PDFF is widely recognized as the most accurate non-invasive biomarker of hepatic steatosis[10-12,21-24]. In our study, we found an excellent correlation (≥ 0.95) between FF estimates on two- and six-point Dixon *vs* MRS-PDFF (P < 0.001). The findings are concordant with the correlations (0.8-0.99) reported in other studies[25-28]. We also demonstrated a strong linear relationship between the Dixon techniques and MRS for liver fat quantification as defined by the equations MRS-PDFF (%) = 4.67 + 0.76 ($FF_{\text{two-point Dixon}}$) and MRS-PDFF (%) = 0.59 + 1.02 ($FF_{\text{six-point Dixon}}$). Findings on ROC analysis demonstrate that the Dixon techniques have excellent accuracy for detecting hepatic steatosis (AUROC ≥ 0.95, P < 0.001)

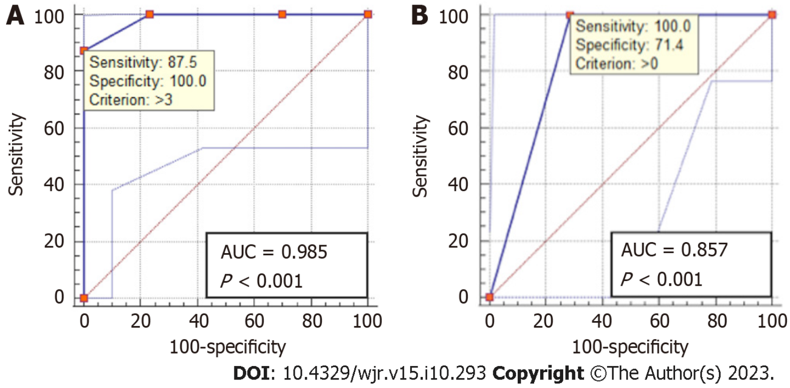

Figure 6 Receiver operating characteristic analysis. A: Receiver operating characteristic (ROC) analysis demonstrates excellent accuracy for grading mild hepatic steatosis on six-point Dixon in patients with no iron overload; B: ROC analysis demonstrates good accuracy for detecting hepatic steatosis on ultrasound. AUC: Area under the curve.

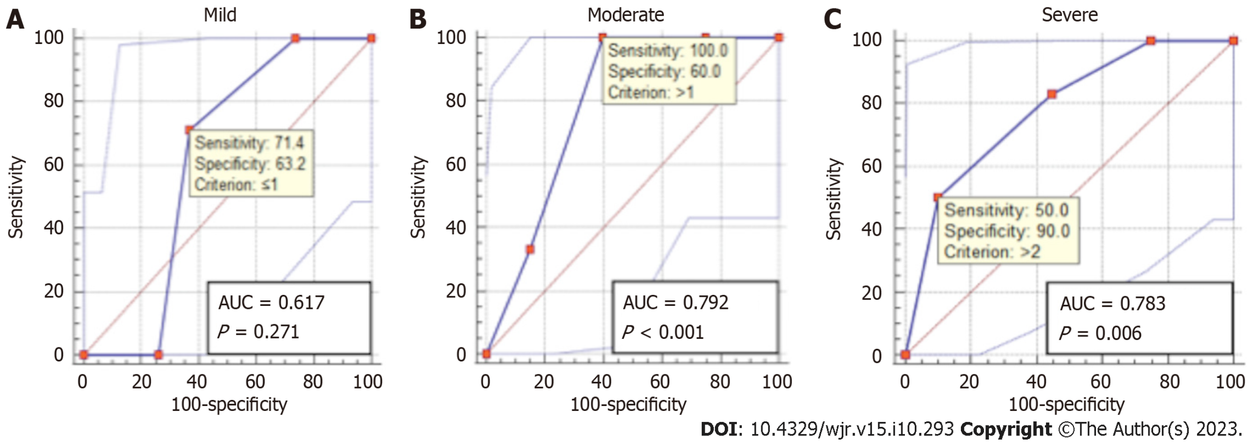

Figure 7 Receiver operating characteristic analysis shows the accuracy for grading mild, moderate and severe hepatic steatosis on ultrasound. A: The accuracy for grading mild hepatic steatosis on ultrasound; B: The accuracy for grading moderate hepatic steatosis on ultrasound; C: The accuracy for grading severe hepatic steatosis on ultrasound. AUC: Area under the curve.

and in grading severe steatosis (AUROC ≥ 0.96, $P < 0.001$) as well as fair accuracy in grading moderate steatosis (AUROC ≥ 0.72, $P = 0.001$). Two-point Dixon also showed fair accuracy for grading mild steatosis (AUROC = 0.75, $P < 0.01$). However, the main limitation of two-point Dixon is that it cannot be used to estimate the FF in iron overload. Despite this, two-point Dixon, a ubiquitous abdominal MR sequence, has the notable practical advantage of being widely available clinically worldwide unlike six-point Dixon or MRS, where clinical access is limited to a number of large specialized centres. In many centers that do not have access to the latter, two-point Dixon may be used as a pragmatic option (''a poor man's fat quantification'') in the absence of iron overload. Moreover, FF estimates on two-point Dixon are technically simple to perform manually and have excellent inter-reader agreement (0.99, $P < 0.001$). In comparison, six-point Dixon can be used in iron overload although subgroup analysis suggests that this test performs better in patients without iron overload. Comparing FF estimates *vs* MRS-PDFF, inter-test correlation was moderate (0.82) in patients with iron overload *vs* excellent (0.97) in patients without iron overload, $P < 0.001$. Bland Altman showed a slightly wider inter-test disparity between FF estimates *vs* MRS-PDFF in patients with iron overload (mean difference = 1.5%, LOA of -9.5%, 12.5%) compared to patients without iron overload (mean difference = 0.7%, LOA of -3.3%, 4.7%). Iron overload also negatively affected the accuracy of six-point Dixon in grading mild steatosis. When patients with iron overload were removed from the analysis, the AUROC increased from 0.59 to 0.99 ($P < 0.001$). Unlike iron overload, liver fibrosis did not affect the correlation between FF estimates on the Dixon techniques and MRS-PDFF. Correlation remained excellent (> 0.9) whether fibrosis was present or absent, $P < 0.01$. Inter-test variability on Bland Altman was similar in patients with or without fibrosis.

US had a poorer diagnostic performance in evaluating hepatic steatosis compared to MRI. The inter-reader agreement was moderate on US *vs* excellent on the Dixon techniques. The accuracy for detecting steatosis was also lower on US (AUROC = 0.86, $P < 0.001$) compared to the Dixon techniques (AUROC ≥ 0.95, $P < 0.001$). Similarly, US had a lower accuracy (AUROC = 0.78, $P < 0.01$) than the Dixon techniques (AUROC ≥ 0.96, $P < 0.001$) in grading severe steatosis.

The study had several limitations. This was a single-center retrospective analysis performed on a relatively modest number of patients. Notwithstanding, the study was adequately powered to detect statistically significant differences. Future multi-institution studies are necessary to determine the generalizability of our findings. Our study cohort was drawn from patients with suspected diffuse parenchymal liver disease, of which 75.8% had hepatic steatosis on MRS-PDFF. While the high prevalence of steatosis in the study provided a valuable source of data for analysis, we acknowledge that our study is skewed by selection bias and does not reflect the true prevalence of steatosis in the general population. Finally, our study was performed exclusively on a single vendor 1.5-T MR platform using clinically available proprietary software. We did not evaluate the confounding effects of higher magnet strengths (*e.g.*, 3-T), different manufacturer platforms, software or protocols as it was not within the scope of our study. An *ex-vivo* phantom study reported that multi-echo Dixon techniques were accurate and reliable across 1.5-T and 3-T, different clinical platforms and multiple institutions[29]. However, a similar study in a large patient population with various grades of hepatic steatosis would be helpful to establish the clinical translatability of the findings.

CONCLUSION

In conclusion, our study findings suggest that in general the Dixon techniques perform satisfactorily for the detection, quantification and grading of hepatic steatosis but with exceptions. Two-point Dixon is a clinically widely available 1st generation technique while six-point Dixon is a modern technique that is not routinely available clinically in many centers. The main weakness of two-point Dixon is that it cannot be used in iron overload due to unmitigated signal decay from T2* effects[30]. In comparison, six-point Dixon can be used in iron overload, although its ability to grade mild steatosis may be compromised suggesting imperfect confounder correction. Additionally, liver fibrosis did not appear to have an impact on FF estimates on the Dixon techniques - a finding that to our knowledge has not been previously reported. Lastly, both Dixon techniques showed superior inter-reader agreement and accuracy for detecting steatosis compared to US. Ability to grade severe steatosis was also better on MR.

ARTICLE HIGHLIGHTS

Research background

Hepatic steatosis is a global healthcare concern.

Research motivation

There is a clinical need to determine how good existing magnetic resonance (MR) techniques are in evaluating hepatic steatosis.

Research objectives

The primary objective was to test the diagnostic performance of two- and six-point Dixon MR techniques in evaluating hepatic steatosis.

Research methods

A retrospective single center study was performed in patients with suspected diffuse parenchymal liver disease. All patients underwent MR imaging assessment with two-point Dixon, six-point Dixon and MR spectroscopy. Findings on two-point Dixon and six-point Dixon were compared against the reference standard, MR spectroscopy.

Research results

We found an excellent correlation (≥ 0.95) between fat fraction estimates on two- and six-point Dixon when compared against magnetic resonance spectroscopy ($P < 0.001$).

Research conclusions

Two- and six-point Dixon are useful MR techniques for evaluating patients with hepatic steatosis.

Research perspectives

MR techniques can provide accurate non-invasive assessment of hepatic steatosis.

FOOTNOTES

Author contributions: Elfaal M, Supersad A, Ferguson C, Locas S, Manolea F, Wilson MP, Sam M, Tu W, and Low G contributed to data collection, data analysis, editing the manuscript; and all authors approved the final manuscript.

Institutional review board statement: The study was reviewed and approved by the Ethics Committee of the University of Alberta, Canada and the Institutional Review Board of Alberta Health Services and Northern Alberta Clinical Trials and Research Centre.

Informed consent statement: The Ethics Committee of the University of Alberta, Canada, waived the requirement for signed informed consent for this retrospective study for which anonymous clinical data was used.

Conflict-of-interest statement: All the authors report no relevant conflicts of interest for this article.

Data sharing statement: No additional data is available.

Country/Territory of origin: Canada

ORCID number: Mitchell P Wilson 0000-0002-1630-5138; Medica Sam 0000-0002-3962-633X; Gavin Low 0000-0002-4959-8934.

S-Editor: Wang JJ
L-Editor: A
P-Editor: Zhao S

REFERENCES

1 **Starekova J**, Reeder SB. Liver fat quantification: where do we stand? *Abdom Radiol (NY)* 2020; **45**: 3386-3399 [PMID: 33025153 DOI: 10.1007/s00261-020-02783-1]

2 **Byrne CD**, Targher G. NAFLD: a multisystem disease. *J Hepatol* 2015; **62**: S47-S64 [PMID: 25920090 DOI: 10.1016/j.jhep.2014.12.012]

3 **Estes C**, Razavi H, Loomba R, Younossi Z, Sanyal AJ. Modeling the epidemic of nonalcoholic fatty liver disease demonstrates an exponential increase in burden of disease. *Hepatology* 2018; **67**: 123-133 [PMID: 28802062 DOI: 10.1002/hep.29466]

4 **Perumpail BJ**, Khan MA, Yoo ER, Cholankeril G, Kim D, Ahmed A. Clinical epidemiology and disease burden of nonalcoholic fatty liver disease. *World J Gastroenterol* 2017; **23**: 8263-8276 [PMID: 29307986 DOI: 10.3748/wjg.v23.i47.8263]

5 **Younossi ZM**, Koenig AB, Abdelatif D, Fazel Y, Henry L, Wymer M. Global epidemiology of nonalcoholic fatty liver disease-Meta-analytic assessment of prevalence, incidence, and outcomes. *Hepatology* 2016; **64**: 73-84 [PMID: 26707365 DOI: 10.1002/hep.28431]

6 **Starekova J**, Hernando D, Pickhardt PJ, Reeder SB. Quantification of Liver Fat Content with CT and MRI: State of the Art. *Radiology* 2021; **301**: 250-262 [PMID: 34546125 DOI: 10.1148/radiol.2021204288]

7 **Bravo AA**, Sheth SG, Chopra S. Liver biopsy. *N Engl J Med* 2001; **344**: 495-500 [PMID: 11172192 DOI: 10.1056/NEJM200102153440706]

8 **Ratziu V**, Charlotte F, Heurtier A, Gombert S, Giral P, Bruckert E, Grimaldi A, Capron F, Poynard T; LIDO Study Group. Sampling variability of liver biopsy in nonalcoholic fatty liver disease. *Gastroenterology* 2005; **128**: 1898-1906 [PMID: 15940625 DOI: 10.1053/j.gastro.2005.03.084]

9 **Cleveland E**, Bandy A, VanWagner LB. Diagnostic challenges of nonalcoholic fatty liver disease/nonalcoholic steatohepatitis. *Clin Liver Dis (Hoboken)* 2018; **11**: 98-104 [PMID: 30147867 DOI: 10.1002/cld.716]

10 **Roldan-Valadez E**, Favila R, Martínez-López M, Uribe M, Ríos C, Méndez-Sánchez N. In vivo 3T spectroscopic quantification of liver fat content in nonalcoholic fatty liver disease: Correlation with biochemical method and morphometry. *J Hepatol* 2010; **53**: 732-737 [PMID: 20594607 DOI: 10.1016/j.jhep.2010.04.018]

11 **van Werven JR**, Schreuder TC, Aarts EO, Nederveen AJ, Meijer JW, Berends FJ, Janssen IM, Mulder CJ, Jansen PL, Stoker J. Hepatic steatosis in morbidly obese patients undergoing gastric bypass surgery: assessment with open-system 1H-MR spectroscopy. *AJR Am J Roentgenol* 2011; **196**: W736-W742 [PMID: 21606262 DOI: 10.2214/AJR.10.5215]

12 **McPherson S**, Jonsson JR, Cowin GJ, O'Rourke P, Clouston AD, Volp A, Horsfall L, Jothimani D, Fawcett J, Galloway GJ, Benson M, Powell EE. Magnetic resonance imaging and spectroscopy accurately estimate the severity of steatosis provided the stage of fibrosis is considered. *J Hepatol* 2009; **51**: 389-397 [PMID: 19505740 DOI: 10.1016/j.jhep.2009.04.012]

13 **Dixon WT**. Simple proton spectroscopic imaging. *Radiology* 1984; **153**: 189-194 [PMID: 6089263 DOI: 10.1148/radiology.153.1.6089263]

14 **Dyke JP**. Quantitative MRI Proton Density Fat Fraction: A Coming of Age. *Radiology* 2021; **298**: 652-653 [PMID: 33475469 DOI: 10.1148/radiol.2020204356]

15 **Reeder SB**, Sirlin CB. Quantification of liver fat with magnetic resonance imaging. *Magn Reson Imaging Clin N Am* 2010; **18**: 337-357, ix [PMID: 21094444 DOI: 10.1016/j.mric.2010.08.013]

16 **Hong CW**, Cui JY, Batakis D, Xu Y, Wolfson T, Gamst AC, Schlein AN, Negrete LM, Middleton MS, Hamilton G, Loomba R, Schwimmer JB, Fowler KJ, Sirlin CB. Repeatability and accuracy of various region-of-interest sampling strategies for hepatic MRI proton density fat fraction quantification. *Abdom Radiol (NY)* 2021; **46**: 3105-3116 [PMID: 33609166 DOI: 10.1007/s00261-021-02965-5]

17 **Saadeh S**, Younossi ZM, Remer EM, Gramlich T, Ong JP, Hurley M, Mullen KD, Cooper JN, Sheridan MJ. The utility of radiological imaging in nonalcoholic fatty liver disease. *Gastroenterology* 2002; **123**: 745-750 [PMID: 12198701 DOI: 10.1053/gast.2002.35354]

18 **Rodge GA**, Goenka MK, Goenka U, Afzalpurkar S, Shah BB. Quantification of Liver Fat by MRI-PDFF Imaging in Patients with Suspected Non-alcoholic Fatty Liver Disease and Its Correlation with Metabolic Syndrome, Liver Function Test and Ultrasonography. *J Clin Exp Hepatol* 2021; **11**: 586-591 [PMID: 34511820 DOI: 10.1016/j.jceh.2020.11.004]

19 **Landis JR**, Koch GG. The measurement of observer agreement for categorical data. *Biometrics* 1977; **33**: 159-174 [PMID: 843571]

20 **Guglielmo FF**, Venkatesh SK, Mitchell DG. Liver MR Elastography Technique and Image Interpretation: Pearls and Pitfalls. *Radiographics* 2019; **39**: 1983-2002 [PMID: 31626569 DOI: 10.1148/rg.2019190034]

21 **Gu J**, Liu S, Du S, Zhang Q, Xiao J, Dong Q, Xin Y. Diagnostic value of MRI-PDFF for hepatic steatosis in patients with non-alcoholic fatty liver disease: a meta-analysis. *Eur Radiol* 2019; **29**: 3564-3573 [PMID: 30899974 DOI: 10.1007/s00330-019-06072-4]

22 **Reeder SB**, Cruite I, Hamilton G, Sirlin CB. Quantitative Assessment of Liver Fat with Magnetic Resonance Imaging and Spectroscopy. *J Magn Reson Imaging* 2011; **34**: 729-749 [PMID: 22025886 DOI: 10.1002/jmri.22775]

23 **Szczepaniak LS**, Nurenberg P, Leonard D, Browning JD, Reingold JS, Grundy S, Hobbs HH, Dobbins RL. Magnetic resonance spectroscopy to measure hepatic triglyceride content: prevalence of hepatic steatosis in the general population. *Am J Physiol Endocrinol Metab* 2005; **288**: E462-E468 [PMID: 15339742 DOI: 10.1152/ajpendo.00064.2004]

24 **Ajmera V**, Loomba R. Imaging biomarkers of NAFLD, NASH, and fibrosis. *Mol Metab* 2021; **50**: 101167 [PMID: 33460786 DOI: 10.1016/j.molmet.2021.101167]

25 **Kramer H**, Pickhardt PJ, Kliewer MA, Hernando D, Chen GH, Zagzebski JA, Reeder SB. Accuracy of Liver Fat Quantification With Advanced CT, MRI, and Ultrasound Techniques: Prospective Comparison With MR Spectroscopy. *AJR Am J Roentgenol* 2017; **208**: 92-100 [PMID: 27726414 DOI: 10.2214/AJR.16.16565]

26 **Yurdaisik I**, Nurili F. Accuracy of Multi-echo Dixon Sequence in Quantification of Hepatic Steatosis. *Cureus* 2020; **12**: e7103 [PMID: 32231898 DOI: 10.7759/cureus.7103]

27 **Hayashi T**, Saitoh S, Takahashi J, Tsuji Y, Ikeda K, Kobayashi M, Kawamura Y, Fujii T, Inoue M, Miyati T, Kumada H. Hepatic fat quantification using the two-point Dixon method and fat color maps based on non-alcoholic fatty liver disease activity score. *Hepatol Res* 2017; **47**: 455-464 [PMID: 27351583 DOI: 10.1111/hepr.12767]

28 **Idilman IS**, Keskin O, Celik A, Savas B, Elhan AH, Idilman R, Karcaaltincaba M. A comparison of liver fat content as determined by magnetic resonance imaging-proton density fat fraction and MRS versus liver histology in non-alcoholic fatty liver disease. *Acta Radiol* 2016; **57**: 271-278 [PMID: 25855666 DOI: 10.1177/0284185115580488]

29 **Hu HH**, Yokoo T, Bashir MR, Sirlin CB, Hernando D, Malyarenko D, Chenevert TL, Smith MA, Serai SD, Middleton MS, Henderson WC, Hamilton G, Shaffer J, Shu Y, Tkach JA, Trout AT, Obuchowski N, Brittain JH, Jackson EF, Reeder SB; RSNA Quantitative Imaging Biomarkers Alliance PDFF Biomarker Committee. Linearity and Bias of Proton Density Fat Fraction as a Quantitative Imaging Biomarker: A Multicenter, Multiplatform, Multivendor Phantom Study. *Radiology* 2021; **298**: 640-651 [PMID: 33464181 DOI: 10.1148/radiol.2021202912]

30 **Colgan TJ**, Zhao R, Roberts NT, Hernando D, Reeder SB. Limits of Fat Quantification in the Presence of Iron Overload. *J Magn Reson Imaging* 2021; **54**: 1166-1174 [PMID: 33783066 DOI: 10.1002/jmri.27611]

Published by **Baishideng Publishing Group Inc**
7041 Koll Center Parkway, Suite 160, Pleasanton, CA 94566, USA
Telephone: +1-925-3991568
E-mail: bpgoffice@wjgnet.com
Help Desk: https://www.f6publishing.com/helpdesk
https://www.wjgnet.com